

Weathering without realizing inorganic CO₂ removal revealed through base cation monitoring.

Arthur Vienne¹, Patrick Frings², Jet Rijnders¹, Lucilla Boito¹, Jens Hartmann³, Harun Niron¹, Reinaldy P. Poetra³, Miguel Portillo Estrada¹, Tom Reershemius⁶, Laura Steinwider¹, Tim Jesper Suhrhoff^{4,5}, Sara Vicca¹

¹Biobased Sustainability Engineering (SUSTAIN), Department of Bioscience Engineering, University of Antwerp, Antwerp, Belgium

²GFZ German Research Centre for Geosciences, Section Earth Surface Geochemistry, Telegrafenberg, 14473 Potsdam, Germany

³Institute for Geology, Centre for Earth System Research and Sustainability (CEN), Universität Hamburg, Bundesstraße 55, 20146 Hamburg, Germany

⁴Yale Center for Natural Carbon Capture, Yale University, New Haven, CT 06511, USA

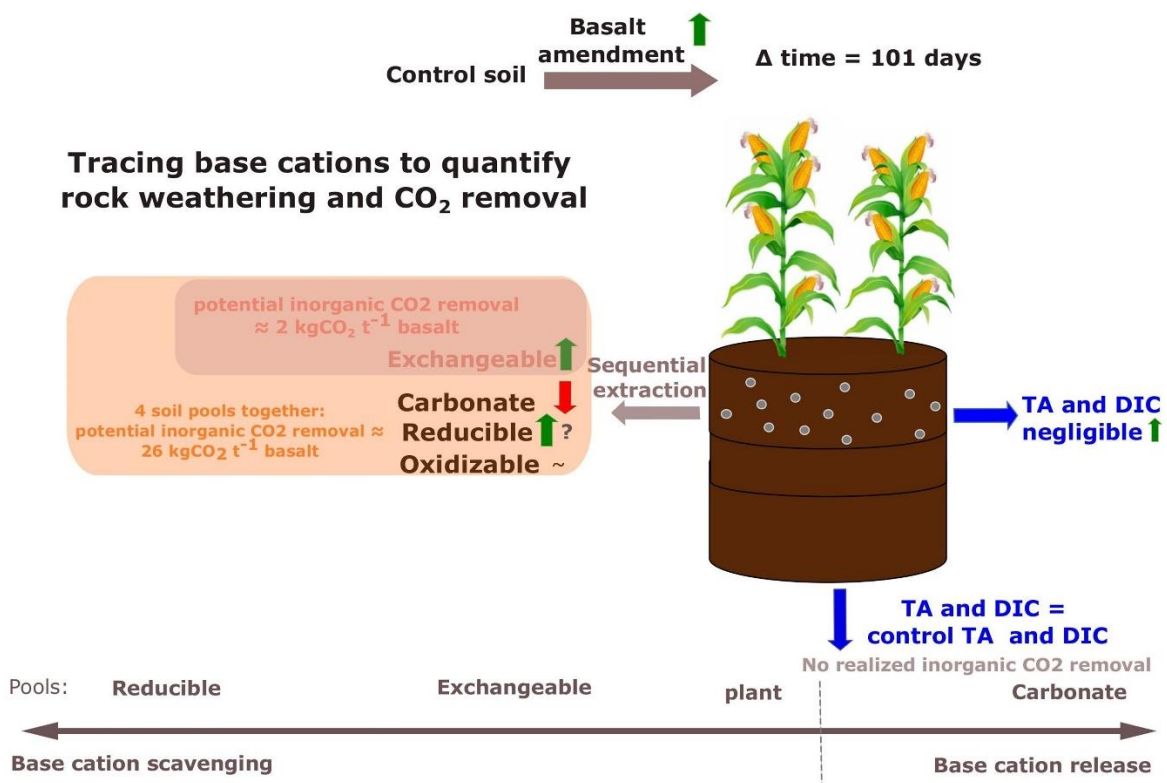
⁵Department of Earth and Planetary Sciences, Yale University, New Haven, CT 06511, USA

⁶School of Natural and Environmental Sciences, Newcastle University, Newcastle upon Tyne, UK

Correspondence to: Arthur Vienne and Sara Vicca arthur.vienne@uantwerpen.be & sara.vicca@uantwerpen.be

Keywords: CDR, Enhanced weathering, Monitoring reporting and verification (MRV), sequential extractions, weathering, basalt, time lags for CO₂ removal, secondary minerals

Graphical abstract



Abstract

Enhanced Weathering using basalt rock dust is a scalable carbon dioxide removal (CDR) technique, but quantifying rock weathering and CDR rates poses a critical challenge. Here, we investigated realized inorganic CO₂ removal (defined as the sum of the change in dissolved inorganic C leaching and in neofomed solid inorganic C) and weathering rates by treating mesocosms planted with maize with basalt (0, 10, 30, 50, 75, 100, 150 and 200 t ha⁻¹) and monitoring them for 101 days. We observed no significant realized inorganic CO₂ removal, as leaching of dissolved inorganic carbon did not increase and soil carbonate content declined over time.

To gain insights into the weathering processes, we traced the fate of base cations in the soil and plants. This analysis showed that most base cations were retained in the topsoil reducible pool, typically associated with iron

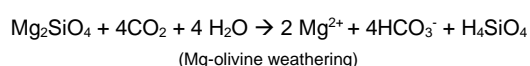
32 (hydr)oxides, while increases in the exchangeable pool were about a factor 10 smaller. Soil base cation scavenging
33 exceeded plant scavenging by approximately two orders of magnitude. From the base cations in all pools (soil, soil
34 water and plants), we quantified log weathering rates of $-11 \text{ mol total alkalinity m}^{-2} \text{ basalt s}^{-1}$. The potential inorganic
35 CO_2 removal, defined as the maximum inorganic CO_2 removal achievable if all weathered base cations, adsorbed
36 by soil pools in this experiment, would leach out of the soil and be fully balanced by carbonate anions, was
37 estimated at $26 \text{ kg CO}_2 \text{ t}^{-1} \text{ basalt}$.

38 In conclusion, despite clear weathering of basalt rock, we found no inorganic CO_2 removal within the timescale of
39 this experiment. The observed increase of aluminum in association with the reducible soil fraction indicate the
40 formation of secondary minerals. These, along with enhanced base cation exchange, may contribute to long-term
41 soil fertility and promote the stabilization of soil organic matter.

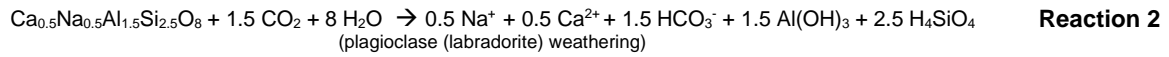
42 **1. Introduction**

43 To meet the "well below 2°C warming" target established by the United Nations' Paris Agreement, Carbon Dioxide
44 Removal (CDR) must complement conventional climate change mitigation efforts (Minx et al., 2018). One CDR
45 technology under consideration is enhanced weathering (EW). EW relies on accelerating natural weathering
46 reactions of silicate minerals with water (H_2O) and carbon dioxide (CO_2) (as in **Reactions 1 to 3**), which increases
47 the concentration of base cations and dissolved inorganic C (DIC) in water, delivering inorganic CO_2 removal. In
48 this study, rather than aiming to quantify a full greenhouse gas budget, we focus on DIC export from soils to the
49 ocean. This pathway is considered the most durable form of carbon sequestration, storing C on timescales
50 exceeding those required for climate change mitigation (Phil Renforth & Henderson, 2017; Berner, 1991).

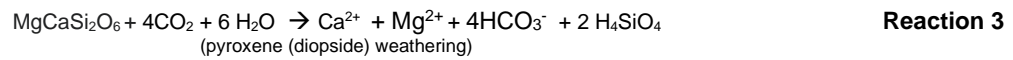
51 DIC (the sum of aqueous $[\text{CO}_2]$, $[\text{HCO}_3^-]$ and $[\text{CO}_3^{2-}]$) can either be measured directly or estimated indirectly from
52 total alkalinity (TA) or electrical conductivity, which are less expensive to monitor and can be empirically linked with
53 DIC through calibration curves (Amann & Hartmann, 2022) (see also **Fig. S10**). This calibration is feasible because,
54 according to the explicit conservative expression for TA in water, $\text{TA} = [\text{HCO}_3^-] + [\text{CO}_3^{2-}] + [\text{OH}^-] - [\text{H}^+]$ (Bijma et
55 al., 2026; Wolf-Gladrow et al., 2007). TA can also be approximated from the sum of base cation charges, minus the
56 sum of conservative anion charges (e.g. chloride, sulphate, phosphate, nitrate) (Barker, 2013; Wolf-Gladrow et al.,
57 2007). DIC can also precipitate as soil inorganic carbon (SIC) in the form of solid carbonates, thereby losing half of
58 the initially captured CO_2 (**Reaction 4**) (Haque et al., 2019). Inorganic CO_2 removal can be defined as the sum of
59 changes in DIC leaching from a soil system after rock amendment plus the change in solid inorganic C (SIC) within
60 the soil system after rock amendment. A robust and reliable accounting of Inorganic CO_2 removal must thus include
61 both monitoring of DIC leaching and SIC changes.



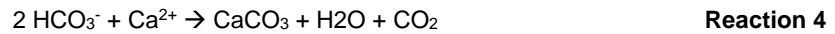
Reaction 1



Reaction 2



Reaction 3



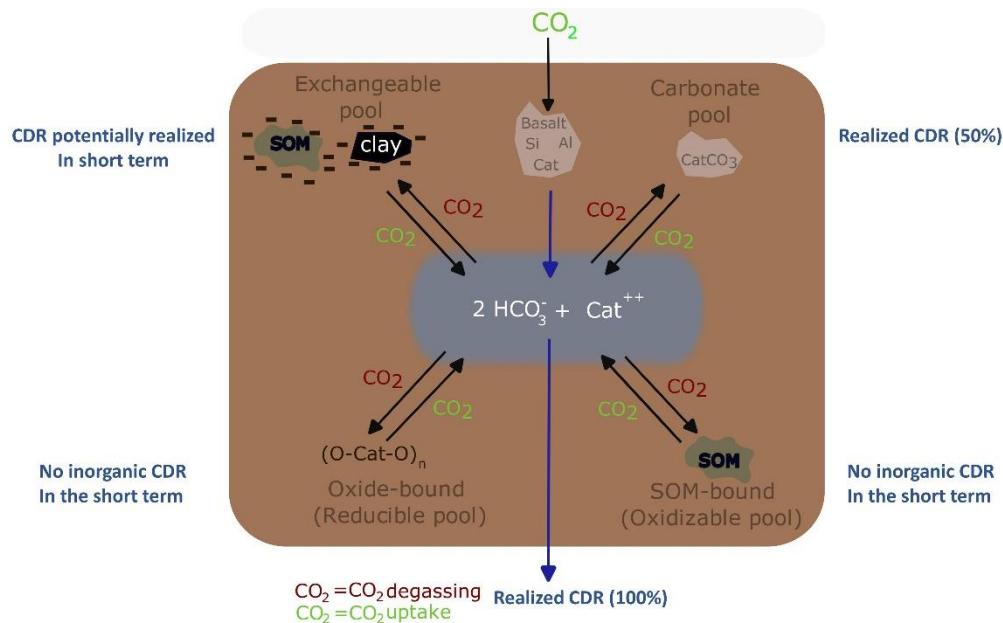
Reaction 4

62 EW is an attractive CDR technology for several reasons. First, EW may provide long-lived to permanent CO₂
63 sequestration: if fixed, DIC is transported via rivers or groundwater to oceans where it may not be released back
64 into the atmosphere for millennia, the timescale needed for oceanic carbonate precipitation, which would release
65 50% of the DIC input back into the atmosphere (**Reaction 4**) (Renforth & Henderson, 2017). Secondly, rock dust
66 amendment has the potential to improve soil fertility and counters soil acidification (Swoboda et al., 2021; Van
67 Straaten, 2006). Thirdly, unlike some other CDR technologies (such as bio-energy with carbon capture and storage
68 or afforestation), EW avoids competition for land with food production (Fuss et al., 2018; Janssens et al., 2022;
69 Smith et al., 2016). Although several rock types are considered for EW, basalt is typically used in EW field trials
70 and has several advantages. Basalt has relatively high base cation content, particularly of calcium (Ca) and
71 magnesium (Mg), which translates into a high potential for CO₂ removal (Renforth et al., 2019). Additionally, basalt
72 is composed of mafic silicate minerals such as plagioclases, pyroxene, and olivine, known for their relatively high
73 weathering rates (Wr). Furthermore, basalt formations are abundant, widely distributed and close to major
74 economies, making the adoption of EW using basalt scalable. Importantly, basalt is safer for agricultural application
75 compared to ultramafic rocks like dunite due to its lower content of heavy metals such as nickel (Ni) and chromium
76 (Cr) (Beerling et al., 2020).

77 Despite the great potential of terrestrial EW and substantial attention by industry in recent years, monitoring rock
78 weathering and CDR is challenging. Quantification of Inorganic CO₂ removal by EW has often focussed on tracking
79 DIC or alkalinity leaching in porewaters (Holzer et al., 2023; McDermott et al., 2024). However, it is also important
80 to consider DIC in exported soil water (leachates)(Larkin et al., 2022) as changes in DIC during soil water transport
81 are well-established. Numerous studies demonstrated that soil water movement and pH strongly govern DIC
82 dynamics, both in soil research (Öquist et al., 2009; Schindlbacher et al., 2019) and in EW research (Dietzen et al.,
83 2018; Niron et al., 2024; Reynaert et al., 2023; Vienne et al., 2024).

84 Focusing solely on changes in DIC and SIC may however overlook other critical soil processes that impact CDR.
85 Besides the carbonate soil pool, other solid soil pools can also extract base cations from solution (**Figure 1**). These
86 pools (temporarily) trap base cations, preventing DIC leaching and could stabilize soil organic matter (SOM) (Buss
87 et al., 2024). Here, we trace the fate of cations in four different soil pools, to gain better estimates of Wrs and CDR.

88



89

90 **Figure 1:** Schematic representation of aluminosilicate rock weathering and four soil pools that scavenge base
 91 cations (= alkalinity): exchangeable pool, carbonate pool, reducible pool and oxidizable pool. Because of charge
 92 balance, uptake of base cations by these pools releases H⁺ that can reconver bicarbonate (HCO₃⁻) (that was a
 93 priori generated from CO₂ through weathering) into CO₂. Cat⁺⁺ = one divalent base cation or two monovalent base
 94 cations. In each corner, in blue, the significance for CDR is indicated for each of the soil pools. Realized CDR
 95 (100%) means that all alkalinity produced by mineral weathering is fully leached from the soil, achieving the
 96 maximum possible inorganic CO₂ removal for that amount of weathering. In contrast, Realized CDR (50%) accounts
 97 for pedogenic carbonate formation (e.g., Reaction 4), where half of the alkalinity released by weathering is
 98 consumed locally, reducing the inorganic CO₂ removal by 50%.

99 Tracing base cations in soils can be done based on the established methodology of Tessier et al. (1979) in which
 100 cations are partitioned into four operationally defined soil pools; The exchangeable pool, the carbonate pool, the
 101 reducible pool and the oxidizable pool. First, in the exchangeable soil pool, cations interact with negatively charged
 102 clay or SOM surfaces. Exchangeable pool cations form relatively weak chemical bounds in a diffuse layer or with
 103 outer-sphere interactions (Blume et al., 2016). Secondly, the carbonate pool contains carbonates such as calcium
 104 carbonate (CaCO₃) and the C in this pool is reported as SIC. The detection of changes in SIC in basalt amended
 105 soils in short-duration experiments is typically challenging (Kelland et al., 2020; Vienne et al., 2022). Focusing on
 106 carbonate base cations may avoid typical issues with C heterogeneity and detection of relatively small SIC changes.

107 Thirdly, Tessier et al. (1979) operationally defined a reducible soil pool where base cations are associated with iron
 108 (Fe) and manganese (Mn) (hydr)oxides. Dzombak & Morel (1990) modelled adsorption of Mg to hydrous ferric
 109 oxides (FeO(OH)), in which a surface hydroxyl group loses a proton and is replaced by a magnesium ion (FeOOH
 110 + Mg²⁺ ⇌ FeOMg⁺ + H⁺) and thereby decreases solute TA. Fourth, the oxidizable pool where cations are bound
 111 to SOM or sulfides.

112 In the fourth soil pool considered here, the oxidizable pool, SOM can form strong bounds with cations after
 113 deprotonation (Kalinichev et al., 2011; Tipping & Hurley, 1992). SOM can thus scavenge cations in both the
 114 exchangeable and oxidizable pool. The binding strength between SOM and a cation determines whether the cation
 115 resides in the exchangeable or oxidizable pool (as graphically schematized in Blume et al., (2016), Fig. 5.6). Cations

116 in the oxidizable pool are expected to chemically stabilize organic matter due to strong cation bridging and inhibition
117 of decomposing enzymes (Rowley et al., 2018).

118 In conclusion, base cations in these soil pools could decrease solute TA after proton release and hence degas DIC
119 while potentially stabilizing SOM. Last, besides soil pools, also plants can scavenge base cations from solution.
120 Base cations that go to the plant pool can be recycled to the aqueous phase, either through decomposition of plants
121 in the field or through the food chain and sewage system, further complicating base cation mass balancing.

122 The undesirable side-effect of base cation scavenging (by plant/soil pools) is the release of protons to maintain
123 charge balance. This release of protons converts negatively charged DIC (HCO_3^- and carbonate anions (CO_3^{2-})) to
124 H_2CO_3 , which is in equilibrium with gaseous CO_2 ($\text{CO}_3^{2-} + \text{H}^+ \rightarrow \text{HCO}_3^-$ and $\text{HCO}_3^- + \text{H}^+ \rightarrow \text{H}_2\text{CO}_3 \rightleftharpoons \text{H}_2\text{O} + \text{CO}_2$
125 (g)). Hence, inorganic CO_2 removal can be reversed during temporary storage of base cations and realized again
126 when base cations are released back from soil and plant pools into the aqueous phase.

127 From base cations in plant and soil pools, we can thus calculate a 'potential inorganic CO_2 removal', a terminology
128 proposed by Steinwider et al., (2025). This is a maximum quantity of Inorganic CO_2 removal that can be achieved
129 when all cations released through silicate weathering are charge-balanced by bicarbonate/carbonates and leached
130 from soils. Base cation retention in different soil pools results in a temporal decoupling between weathering and
131 inorganic CO_2 removal. The timeframe in which the potential inorganic CO_2 removal can be achieved is a major
132 uncertainty in EW (Kanzaki et al., 2025). For weakly bound exchangeable cations, potential inorganic CO_2 removal
133 may be achieved in the relative short term of decades. Within this timeframe, because of stronger binding strengths,
134 reducible and oxidizable base cations are more unlikely to be released and thus deliver inorganic CO_2 removal.
135 Last, inorganic CO_2 removal is only achieved if the weathering agent that induced the weathering was H_2CO_3 (as
136 in Reaction 1-3). If the weathering agent is another acid (e.g. nitric acid (HNO_3) from fertilizers), no inorganic CO_2
137 removal occurs within the soil (McDermott et al., 2024; Taylor et al., 2021).

138 In a mesocosm experiment with basalt rock powder addition, we aimed to accurately quantify the W_r and potential
139 inorganic CO_2 removal through quantification of base cations in the four abovementioned soil pools, soil water and
140 maize plants. Tracing the fate of alkalinity after its generation by the weathering of primary minerals is key to
141 accurately quantify basalt W_r s. Here, we make a mass balance after 101 days of experiment, investigate the fate
142 of base cations through exploration of sequential extractions as a monitoring strategy for weathering and
143 implications for C sequestration.

144 **2. Materials and Methods**

145 **2.1 experimental set-up**

146 A mesocosm experiment with 30 mesocosms was constructed at the experimental site at the Drie Eiken Campus
147 of the University of Antwerp (Belgium). This experiment was part of a larger mesocosm experiment that aimed to
148 investigate heavy metal fate and plant biomass in silicate amended maize plants (Rijnders et al., 2025). The

149 mesocosms (0.6 m height, radius=0.25m) received natural rainfall and received additional water through manual
 150 irrigation (**Fig. S2**). In May 2021, the lower 40 cm of each mesocosm was filled with a slightly acidic sandy loam
 151 soil (**Table 1**).

152 **Table 1:** Properties of control soil. w%=weight percent.*

Control soil properties		Number of Replicates	Measuring method
pH	5.66 ± 0.01	3x (before addition soil to pots)	(in a soil: water suspension (1:2.5))
Texture (Sand, clay, silt w%)	Sandy loam (61, 4, 35 w%)	3x (before addition soil to pots)	**
Soil organic C (SOC) (w%)	0.53 ± 0.01	4x (0-20 cm)	***
SIC (w%)	0.0031 ± 0.0002	4x (0-20 cm)	carbonate extraction (see Equation S4 in supplement)
Cation exchange capacity (CEC) (meq/100g)	3.03 ± 0.11	15x (3 depths x 5 control pots)	(Brown, 1943)
Base saturation (%)	50 ± 5	15x (3 depths x 5 control pots)	(Brown, 1943)
Bulk density (BD) (kg/L)	1.58±0.02	14x (5x 0-20, 5x 20-30cm 4x 30-50cm)	Sampling soil cores (100 cm ³ , 5 cm length x 20 cm ²). And weigh after drying soil at 70°C for 48 hours
Fe-(hydr)oxide (mg Fe/g soil)	1.13±0.04	12x (4x 0-20, 4x 20-30cm 4x 30-50cm)	^{iv}

153 *Reported values represent the average ± standard error (SE) of control soil after the experimental period of 101 days unless
 154 stated otherwise. ** 40g of air dried soil was shaken for 18 hours with 100 mL of 50 g L⁻¹ sodium hexametaphosphate solution,
 155 sieved over 63 µm to separate sand from silt+clay. The same was done for a blank. The sieved solutions (sample and blank) were
 156 diluted with deionized water to one liter and after six hours density and temperature were measured. Clay = (density (sample) –
 157 density (blank))/ sample mass and silt= 100%-sand%-clay%.***Determined through loss on ignition (4h heating at 360°C and
 158 assuming a SOC/SOM ratio of 0.58 (Van Bemmelen, 1890)). ^{iv} Estimation of the Fe (hydr)oxide content for control soil based on
 159 Fe in the reducible pool (method of extraction: see Table 3).

160 The upper 20 cm was filled with the same soil, either unamended in the control treatment (five mesocosms), or
 161 amended with basalt (**Figure 2**). Five mesocosms received 50 ton basalt ha⁻¹, while six others received different
 162 amounts of basalt, ranging between 10 and 200 ton ha⁻¹ (**Table 2**). The basalt was mixed homogenously in the
 163 control soil using a concrete mixer. Basalt was obtained from DURABAS (<https://www.rpbl.de>). Particle size
 164 distribution (PSD) was analyzed using a mastersizer 2000 with a Hydro 2000G sample dispersion unit after
 165 removing larger particles with a 2 mm sieve. The P80 was 310.78 µm (see **Fig. S5**). The specific surface area
 166 (SSA) was determined with a Quantachrome Autosorb iQ using the Braunauer-Emmet-Teller (BET) method. The
 167 measurement used nitrogen gas as adsorbate with multi-point (5 points) and isotherm (77K) settings. Samples with
 168 the same treatment were pooled in equal quantities into one sample to reduce the cost and time for analysis. All
 169 samples were degassed at 300 °C with 200 minutes of soak time. High measurement quality was ensured by

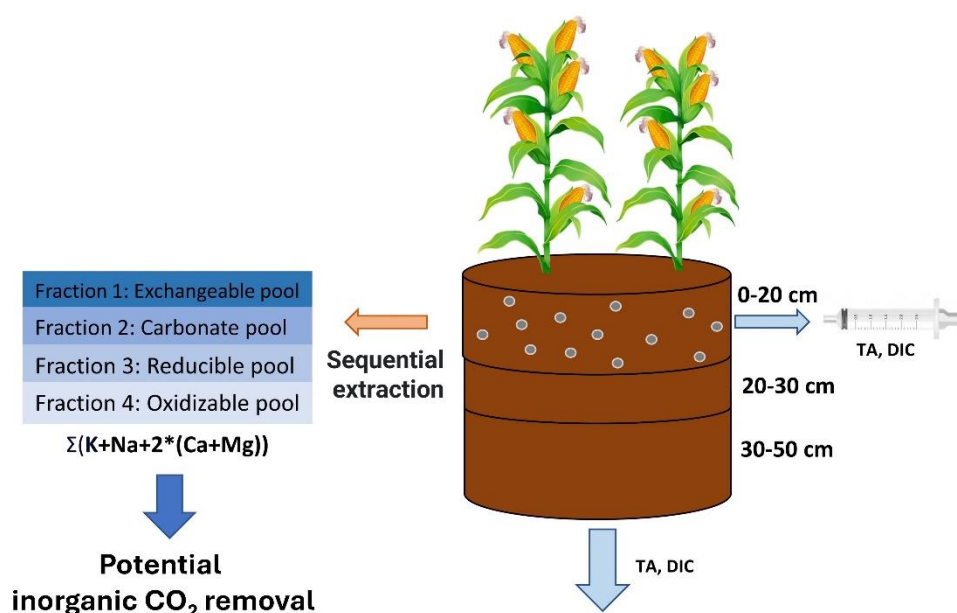
170 frequent reference measurements (Bundesanstalt für Materialforschung und -prüfung, Germany) in addition to three
 171 technical repetitions for each measurement. The BET-SSA of the basalt rock was $9.226 \pm 0.08 \text{ m}^2 \text{ g}^{-1}$. X-ray
 172 diffraction (XRD) and x-ray fluorescence (XRF) analyses are provided in the supplement.

173 **Table 2:** Overview of basalt application rates. The 0 and 50 t basalt ha⁻¹ application rates were replicated in five
 174 mesocosms, while other application rates were only tested in one mesocosm. We added these replicates within
 175 individual application rates to learn about the variability between mesocosms receiving the same treatment.

Ton silicate ha ⁻¹ (replications)	0 (5x)	10	30	50 (5x)	75	100	150	200
---	-----------	----	----	------------	----	-----	-----	-----

176
 177 Basalt was mixed into the top soil on 17/5/2021. To allow leachate collection, mesocosms had a 2 cm diameter
 178 hole at the bottom. On the inside, the bottom of the pot was covered with a root exclusion mesh to prevent soil
 179 export. Glass collectors (2.3L volume) were placed under the mesocosm to collect the leachates. Leachate volumes
 180 were determined throughout the experiment and were collected for chemical analyses on seven occasions. On
 181 3/6/2021, two sweet maize seedlings (variety Tom Thumb) were planted in each the mesocosms and all pots
 182 received fertilization with nitrogen (N), phosphorus (P) and potassium (K) (96 – 10 – 79) kg ha⁻¹ by adding Ca nitrate
 183 (Ca(NO₃)₂), triple super phosphate (TSP, 45% P₂O₅) and potassium sulfate (K₂SO₄). The experimental duration
 184 was 101 days; plants were harvested on 26/8/2021.

185 Soil water content and temperature were recorded using Cambell Scientific sensors (CS616) that are 30 cm in
 186 length. Watering (using rain water collected from a tank) was executed manually and total water manual inputs
 187 were tracked. In addition, daily precipitation amounts (in mm) were obtained for Wilrijk (Belgium) using the open
 188 source tool (visualcrossing.com). In the supplement, an overview of environmental conditions (rainfall, total water
 189 inputs, temperature and soil moisture) is given.



190
 191 **Figure 2:** Overview of experimental set-up and measurements.

192 **2.2 Leachate and pore water analysis**

193 Weekly pore water sampling was performed with rhizons (Rhizon Flex, Rhizosphere Research Products B.V.,
194 Wageningen, NL) installed at 5 cm depth in each mesocosm. Leachate and porewater samples were filtered through
195 a 0.45 µm PET filter. The major cations (Ca, Mg and K) were measured through ICP-OES (iCAP 6300 duo, Thermo
196 Scientific). Na was not directly measured in soil water samples; however, its charge contribution is accounted for
197 indirectly in the measured soil water alkalinity. Before analysis, ICP samples were conserved using 1.5 mL (HNO₃
198 69%) per 30 mL sample. TA was determined using a SAN++ continuous flow analyzer (Skalar - NLD). The pH was
199 measured using a HI3220 pH/ORP meter. Dissolved organic carbon (DOC) and DIC were measured using a
200 FormacsHT with LAS sampler (Skalar - NLD). DIC and DOC were measured on eight and 12 occasions in leachates
201 and pore water respectively.

202 Two quality control (QC) standards were analyzed for individual elements (Ca, K, Mg, sodium (Na), silicon (Si) and
203 Fe). The mean precision of the QC standards was 0.84%, 1.12%, 0.54%, 2.79%, 1.67% and 1.30% for the
204 respective elements. The mean accuracy for the two QC standards was 1.87%, 2.30%, 0.17%, 1.88%, 1.39% and
205 2.65% for Ca, K, Mg, Na, Si and Fe respectively. For TA soil water samples, mean accuracy and precision for two
206 different QC standards were 1.51 and 1.72% respectively. The DIC measurements with FormacsHT had an
207 accuracy and precision 1.09 and 0.23% respectively. Accuracy and precision were determined based on 12
208 measurements of a QC for TA (standards: 150 and 350 mg CaCO₃ L⁻¹) and DIC (range between 10 and 100 mg L⁻¹)
209 and based on eight measurements of two different QC concentrations for each individual element.

210 **2.3 Soil collection and pretreatment**

211 Top soil pH was measured on five dates. To determine top soil pH, 4 g of air dried topsoil sample was dissolved in
212 10 mL deionized water and shaken before pH measurement using a HI3220 pH/ORP meter (Hanna Instruments,
213 Temse, Belgium). After harvesting, soils were sampled using cylindrical soil cores (100 cm³, 5 cm length x 20 cm²).
214 Samples were taken across the depth of the mesocosm and three sampling depths were considered (0-20cm, 20-
215 30cm, 30-50cm). One sample was taken for each depth and mesocosm. The cores were dried at 70°C for 48 hours
216 to determine water content (gH₂O/g soil) and bulk density. An additional soil sample was taken at each depth, dried
217 at 70 °C for 48 hours and used for chemical analyses after sieving over a 2 mm sieve, removing the majority of the
218 root biomass. Estimated base cations in sieved-off roots were negligible relative to soil pools and thus excluded
219 from our main cation budget.

220 **2.4 Sequential base cation extractions**

221 As conceptualized by Tessier et al. (1979), base cations can reside in four different soil pools: the exchangeable
222 pool (cations weakly bound to SOM or clays), the carbonate pool (cations bound in pedogenic carbonates), the
223 reducible pool (cations bound to Al/Mn/Fe hydr(oxide)) and the oxidizable pool (cations strongly bound to SOM).
224 SOM bound to cations, extracted with weak salt solutions in the exchangeable pool typically has a low turnover time

225 (Poeplau et al., 2018) and is therefore thought to be more susceptible to microbial decomposition than oxidizable
 226 SOM.

227 We adapted the original Tessier scheme by replacing 1M magnesium chloride with 1M ammonium acetate
 228 ($\text{NH}_4(\text{CH}_3\text{COO})$) for extraction of the exchangeable pool, in order to be able to measure all base cations in the
 229 exchangeable pool. Likewise, Na-acetate was replaced with a mixture of acetic acid and water to be able to measure
 230 Na in the carbonate pool. We quantified SIC changes from the base cations in these acetic acid extracts (as in
 231 (Larkin et al., 2022)) (see also Equation S4). Additionally, three other SIC measurement techniques were explored
 232 to compare and the sensitivity of detecting SIC changes after amending with a range of basalt (see section S3.7).

233 **Table 3:** Overview of sequential extraction method
 234 (extraction time, temperature, conditions, volume of extractants and chemical composition of extractants).

235	Extraction scheme	Extraction scheme Adapted Tessier et al. (1979)*
236	Pool 1: Exchangeable pool	10 mL 1M $\text{NH}_4(\text{CH}_3\text{COO})$ 1h, 20°C, shaker → centrifuge → sample
237	Pool 2: Carbonate pool	5 mL 1M acetic acid (2h, 20°C, shaker) + 4 mL H ₂ O + 1 mL 3M $\text{NH}_4\text{Acetate}$ → sample
238	Pool 3: Reducible pool	20mL 0.04M hydroxylamine ($\text{NH}_2\text{OH}\cdot\text{HCl}$) in 25% (v/v) acetic acid (pH 2) 6h, 96°C, heat bath
239	Pool 4: Oxidizable pool	3mL 0.02M HNO_3 +5mL 30% peroxide (H_2O_2) (to pH 2 with HNO_3): 2h, 85°C, heat bath +3mL 30% H_2O_2 (to pH 2 with HNO_3) 3h, 85°C, heat bath +5mL 3.2M $\text{NH}_4(\text{CH}_3\text{COO})$ (in 20 vol% HNO_3) +4 mL H ₂ O 0.5h, 20°C, shaker

245 Prior to extractions, approximately 1g of soil was air dried. We also conducted the extractions for the pure basalt
 246 that was initially added to the mesocosms to be able to correct for the cations that were initially already present as
 247 exchangeable, carbonate, reducible and oxidizable pool cations. After each extraction, samples were centrifuged
 248 for 2 minutes at 2000 rpm, supernatants were collected for analysis. The remaining soil pellet after centrifugation
 249 was washed with 10 mL of demineralized water before the following step. Relevant elements (K, Na, Mg, Ca, Al,
 250 Fe and Si) were measured in each pool using ICP-OES (iCAP 6300 duo, Thermo Scientific) for each pool. Si was
 251 only assessed in the reducible pool and in the oxidizable pool to investigate whether Si forms amorphous oxides or
 252 allophane-like compounds or binds with organic matter. Al carbonates were not quantified here as naturally these
 253 carbonates are not commonly formed (Takaya et al., 2019).

254 2.5 Plant responses

255 On 26/8/2021(101 days after basalt amendment in soils), the aboveground biomass was harvested and dried for
 256 48h at 70 °C to determine dry weight. For the results on root biomass we refer to Rijnders et al. (2025)). Plant
 257 material was ground with an ultra-centrifugal mill (Model ZM 200, Retsch GmbH, Haan, Germany). Base cations
 258 (Ca, Mg and K) were measured through ICP-OES (iCAP 6300 duo, Thermo Scientific) in aboveground biomass to

259 calculate plant base cation stocks. Na was not measured in aboveground biomass, because the amount of
260 weathered base cations accumulated in plants is relatively small compared to that in soils, we do not expect this
261 omission to substantially affect our results. Base cations were measured separately in all aboveground biomass
262 parts: stems, leaves, flowers and maize ears.

263 **2.6 Calculation of W_r and potential inorganic CO_2 removal**

264 We use the delta (Δ) symbol to denote the difference relative to unamended control soil. Accordingly, we quantify
265 ΔTA (the change in total alkalinity in the basalt-amended soil relative to the control) based on the difference in base
266 cation concentrations between amended and unamended soils. As basalt only contains cations and no conservative
267 anions, we assume that ΔTA can be quantified from the change in base cation charges (**Equation 1**).

$$268 \quad \Delta\text{TA} \approx 2 * (\Delta\text{Ca} + \Delta\text{Mg}) + \Delta\text{Na} + \Delta\text{K} - \Delta\text{conservative anions} \quad (1)$$

with $\Delta\text{conservative anions} = 0$

269 We thus use a base cation accounting approach as also proposed by Bijma et al. (2026) and explicitly assume no
270 changes in conservative anions after basalt amendment. Still, nitrogen cycling processes (nitrification and
271 denitrification) may be sensitive to soil chemistry and may therefore differ between treatments. Further research is
272 needed to verify whether conservative anions such as nitrates and phosphates are affected by rock amendment.

273 The W_r corresponds to the rate of rock dissolution. The W_r can be expressed per element or as moles of alkalinity
274 equivalents (i.e. the sum of base cation charges (**Equation 1**) per amount of rock surface area per unit of time (in
275 $\text{mol m}^{-2} \text{rock s}^{-1}$). In addition, we calculate a 'potential inorganic CO_2 removal'. We use the same definition for
276 potential inorganic CO_2 removal as in Steinwider et al. (2025). A 'potential inorganic CO_2 removal' can be defined
277 as the maximum amount of inorganic CO_2 that could be removed if all experimentally determined, weathered, soil-
278 retained base cations were to leach from the soil and be completely balanced by carbonate anions. Potential
279 inorganic CO_2 removal was previously 'CDR potential' by Niron et al. (2024)). The concept of CDR potential was
280 first introduced by Phil Renforth (2019) to describe the maximum inorganic CO_2 removal achievable if all base
281 cations within a rock were to completely weather. More recently, Beerling et al., (2024) quantified base cation losses
282 from topsoils using an immobile/mobile tracer approach (see Section 4.2), from which they also derived a measure
283 of CDR potential. To maintain conceptual clarity, we avoid using the term CDR potential for purposes other than its
284 original definition by Renforth (2019). When the term is employed, its meaning should always be explicitly stated.

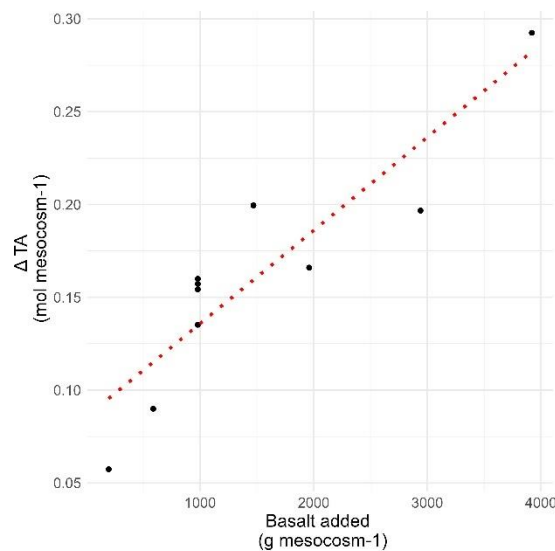
285 To calculate the W_r (from all base cation increases relative to controls in plants, extracted soil fractions and soil
286 water leachates), we sum changes in TA in the following pools: exported soil water (leachates), plants and soil
287 pools. Weathering rates are uncertain due to variability in soil cation pools considered, potential underestimation
288 from unextractable base cations in secondary minerals and methodological limitations in detecting all weathering
289 products. We can express changes in the cation pool of each reservoir as the equivalent W_r required to supply the

290 cations ($W_{leachate}$, W_{plant} and W_{soil}) (**Equation 2**). Conventionally W_{rs} are expressed using a logarithmic scale as
 291 absolute values can vary strongly.

$$292 \quad \text{Log } W_r \left[\frac{\Delta \text{mol TA}}{\text{m}^2 \text{rock.s}} \right] = \text{Log} \left(\frac{\Delta \text{mol TA}_{soil} + \Delta \text{mol TA}_{plant} + \Delta \text{mol TA}_{leachate}}{\text{m}^2 \text{rock.s}} \right) \quad (2)$$

293
 294 We used a gradient of rock applications, where we calculated the slope of the molar change in base cation charges
 295 (expressed as an equivalent “alkalinity” change if these base cations were dissolved in water) with higher rock
 296 amendment (TA slope) (**Figure 3**). We compared logarithmic and linear regression and selected the linear
 297 regression approach, as both approaches had comparable R^2 and Akaike Information Criterion (AIC) values values
 298 and linear slopes ease further data processing (**Fig. S23 and Table S5**). We opted for the linear regression
 299 approach to simplify subsequent calculations. To make our gradient approach more robust, we also calculated the
 300 log W_r for individual application rates in **Fig. S13**.

301



302

303 **Figure 3:** Illustration of the calculation of TA slope: alkalinity scavenging by a given pool was plotted in function of
 304 the applied basalt, and the resulting slope was used to quantify the weathering rate (W_r). This figure is an example
 305 regression with data for the top soil exchangeable pool. All regressions can be found in **Fig. S22**. Normalizing for
 306 mean control alkalinity equivalents before regression shifts the intercepts in Fig. S22 but does not affect the slope,
 307 preserving the relationship between basalt addition and the response variable (Gelman & Hill, 2007).

308 Then we converted units of the alkalinity slope for increasing rock application (TA slope) per unit of rock mass to
 309 moles of alkalinity per rock surface area and per time (**Equation 3**). Equation 3 was used to calculate $\Delta \text{mol TA m}^{-2}$
 310 rock s^{-1} of base cations in leachates, plants and of every measured soil pool at every soil depth.

$$311 \quad \frac{\Delta \text{mol TA}}{\text{m}^2 \text{rock.s}} = \frac{\text{Scavenged alkalinity (= TA slope)} \left[\frac{\Delta \text{mol TA}}{\text{g rock}} \right]}{\text{Experimental duration [s]} * \text{SSA}_{\text{silicate}} \left[\frac{\text{m}^2 \text{surface area}}{\text{g rock}} \right]} \quad (3)$$

312 $\Delta\text{mol TA m}^{-2} \text{ rock s}^{-1}$ was thus quantified per pool, based on the change in base cations in the basalt treatment
 313 compared to the control treatment. For plants, we calculate TA slope through regression of harvested base cations
 314 with basalt application. Harvested base cations were calculated as the product of harvested aboveground biomass
 315 and their base cation content. Charge contributions of Na were not included; Na was not quantified at the time of
 316 plant biomass elemental analysis, which may lead to an underestimation of the alkalinity equivalent increase in the
 317 plant pool. However, given that base cation charges in the plant pool were about two orders of magnitude smaller
 318 than in the soil pool, we expect the effect of this omission to be limited. In addition, maize plants aim to actively
 319 increase their K/Na ratio which avoids salt stress, the K content of maize shoots is typically about 2 orders of
 320 magnitude larger than Na (Gao et al., 2016; Suarez & Grieve, 1988). For leachates, TA slope was calculated as
 321 the product of mean cumulative leachate volume and mean leachate TA concentration for each application rate and
 322 regressing them with the applied basalt as dependent variable.

323 Finally, the W_r attributable to the change in cation content of the soil pools ($W_{r\text{soil}}$) was calculated by summing the
 324 $W_{r\text{soil,layer } k, \text{pool } j}$ for each pool and depth (**Equation 4**). Here, we sum changes in all pools of the topsoil (0-20 cm)
 325 and lower depths (20-30 cm and 30-50 cm) to obtain an aggregate value for $W_{r\text{soil}}$. With
 326 $W_{r\text{soil,layer } k, \text{fraction } j}$ calculated as in **Equation 4** (with k = the number of depths and j = the number of considered
 327 soil pools). TA slope at every depth and soil pool was calculated as in **Equation 5**.

$$328 \quad W_{r\text{soil}} = \sum_{k=1}^3 \sum_{j=1}^4 W_{r\text{soil,layer } k, \text{pool } j} \quad (4)$$

$$329 \quad \text{scavenged TA (TA slope)} \left[\frac{\Delta\text{mol}}{\text{g rock}} \right] = \frac{\frac{\mu\text{mol TA}}{\text{g dry Soil}} (\text{Amended Soil}) - \frac{\mu\text{mol TA}}{\text{g dry Soil}} (\text{control Soil})}{\text{Application rate (Amended soil)} \left[\frac{\text{g rock m}^{-2} \text{ ground area}}{\text{m}^2} \right] * 1000} * \text{Bulk Density} \left[\frac{\text{kg dry Soil}}{\text{m}^3 \text{ soil}} \right] * \text{thickness soil layer [m]} \quad (5)$$

330 Equivalents of soil retained base cation charge equivalents per gram of dry soil mixture can be calculated for each
 331 mesocosm by summing the charges from each base cation (**Equation 6**).

$$332 \quad \frac{\mu\text{mol TA}}{\text{g dry Soil}} = \sum_{j=1}^4 \left(\frac{\frac{\mu\text{g Ca}_{\text{pool } j}}{\text{g dry soil}}}{40.078 \frac{\text{gCa}}{\text{molCa}}} + \frac{\frac{\mu\text{g Mg}_{\text{pool } j}}{\text{g dry soil}}}{24.305 \frac{\text{gMg}}{\text{molMg}}} \right) * \frac{2\text{mol TA}}{\text{mol cat}^{++}} + \left(\frac{\frac{\mu\text{g Na}_{\text{pool } j}}{\text{g dry soil}}}{22.990 \frac{\text{gNa}}{\text{molNa}}} + \frac{\frac{\mu\text{g K}_{\text{pool } j}}{\text{g dry soil}}}{39.098 \frac{\text{gK}}{\text{molK}}} \right) * \frac{1\text{mol TA}}{\text{mol cat}^+} \quad (6)$$

333 These individual base cations (e.g. Ca in pool j) are calculated from the difference of cations weathered during the
 334 weathering operation minus the cations initially present in that fraction in the applied feedstock (Power et al., 2025)
 335 (**Equation 7**). For example, some cations can already exchange on the surface or edges of the applied minerals,
 336 so that these cannot be counted as weathered, they will however contribute to CDR once leached.

337 To calculate in-situ W_r , it is thus necessary to correct for the cations that had already been weathered from primary
 338 minerals at the time of silicate amendment. This correction is typically currently not being done in EW literature yet.

339 As basalt is only added to the top soil and not deeper, this correction is only done for the 0-20 cm soil layer here.
 340 A limitation of the approach in Equation 7 is that it assumes no physical transport of basalt to deeper soil layers,
 341 which may lead to underestimating weathered base cations in the 0–20 cm layer and overestimating them in the
 342 20–30 cm layer.

$$343 \quad \frac{\mu\text{g element}_{i_{poolj}}}{\text{g dry soil}} = \left(\frac{\mu\text{g element}_{i_{poolj}}}{\text{g dry soil}} \right)_{\text{Post weathering, soil mixture}} - \left(\frac{\mu\text{g element}_{i_{poolj}}}{\text{g dry soil}} \right)_{\text{added with feedstock initially}} \quad (7)$$

344 The mass of a specific element (i) in each of the four (j) soil pools (in $\mu\text{g element/g soil}$) is calculated using **Equation**
 345 **8**.

$$346 \quad \left(\frac{\mu\text{g element}_{i_{poolj}}}{\text{g dry soil}} \right)_{\text{Post weathering, soil mixture}} = \frac{\text{concentration element}_i \text{ in pool}_j \left[\frac{\text{mg}}{\text{L}} \right] * \text{Volume extract}_j [\text{mL}]}{\text{mass of solid extracted} [\text{g}]} \quad (8)$$

347 The initial addition of element i to pool j is calculated as in **Equation 9**.

$$348 \quad \left(\frac{\mu\text{g element}_{i_{poolj}}}{\text{g dry soil}} \right)_{\text{added with feedstock initially}} = \frac{\mu\text{g element}_i \text{ pool}_j}{\text{g silicate}} * \frac{\text{Application rate} \left[\frac{\text{g silicate}}{\text{m}^2} \right]}{\text{Bulk density} \left[\text{g dry soil} \frac{\text{soil}}{\text{m}^3} \right] * \text{depth of soil amendment} [\text{m}]} \quad (9)$$

349 According to the charge balance (**Reaction 1-3**) during mineral dissolution, 1 mol HCO_3^- mol⁻¹ TA is generated (and
 350 thus 1 mol of CO_2 is sequestered). We define a factor η , that is equal to the ratio of HCO_3^- per mol of generated
 351 TA. According to charge balance, $\eta=1$. A more conservative approach is to assume that all this generated alkalinity
 352 will be exported to the ocean, after which chemical equilibrium degasses a portion of the alkalinity ($\eta = 0.7$ mol CO_2
 353 mol⁻¹ TA, assumed for oceans) (Renforth et al., 2012; Renforth et al., 2019; Renforth & Henderson, 2017).
 354 According to Renforth et al. (2019), the ocean alkalization efficiency η ranged between 0.7 and 0.85. This η
 355 parameter is relatively uncertain given that model studies indicate that η can range between 0.65 and 0.8 mol CO_2
 356 mol TA⁻¹ (see section S6 in the supplement of (Kowalczyk et al., 2024)). Alternatively, we can assume that all base
 357 cations will form solid carbonates in soils or rivers. In this case $\eta=0.5$ mol CO_2 mol⁻¹ TA (**Reaction 4**). In **Table 4**,
 358 we calculated potential inorganic CO_2 removals assuming conservative values of $\eta=0.5$ (carbonate precipitation
 359 scenario) and $\eta=1$ (the highest possible η without any downstream DIC losses).

360 While calculating W_r , cations added with the rock feedstock that were already weathered were subtracted as in
 361 **Equation 7**, yet these cations are not subtracted to calculate the potential inorganic CO_2 removal as base cations
 362 in weathered fractions of the rock feedstock can also leach to soil water whereby HCO_3^- is generated. Last, base
 363 cation changes in the plant pool were excluded from the potential inorganic CO_2 removal pool here, as a
 364 conservative approach we assume that base cations in plants will not reach the ocean. The latter assumption had
 365 a negligible impact on the potential inorganic CO_2 removal estimate (**Table 4**).

$$366 \quad \text{potential inorganic CO}_2 \text{ removal} \left[\frac{\text{kg CO}_2}{\text{t rock}} \right] = \text{Scavenged TA} \left[\frac{\text{mol TA}}{\text{g rock}} \right] * \frac{\eta \text{ mol CO}_2}{\text{mol TA}} * \frac{44\text{gCO}_2}{\text{mol CO}_2} * 1000 \quad (10)$$

with $\left(\frac{\mu\text{g element}_{i_{poolj}}}{\text{g dry soil}} \right)_{\text{added with feedstock initially}} = 0$

367

368

369 **2.7 Calculation of the carbonate saturation indices (SI_c) using Phreeqc**

370 To assess whether carbonate precipitation was theoretically possible during this experiment, we calculated SI_c for
371 dolomite and calcite. For Mg and Ca the SI_c as the logarithm of the ion activity product and the solubility product
372 constant if dolomite and calcite (SI_c = log IAP/K). Minerals have the potential to precipitate when a log SI_c >0 is
373 reached although substantial oversaturation of calcite (log SI_c > 1) without calcite formation is possible in rivers due
374 to ion inhibition, e.g. by phosphate (Morse et al., 2007; Zhang et al., 2022). Likewise, they are in equilibrium at a
375 log SI_c =0 and dissolve if log SI_c <0. The R phreeqc package was used and the phreeqc.dat database was used.
376 As an input, the experimental pore water (10 cm depth) composition of Mg and Ca was entered, as well as measured
377 pH and TA. Daily SI_c values were calculated by feeding unique combinations of Mg, Ca, pH and into the PHREEQC
378 solution function for each day.

379

380 **2.8 Data analysis**

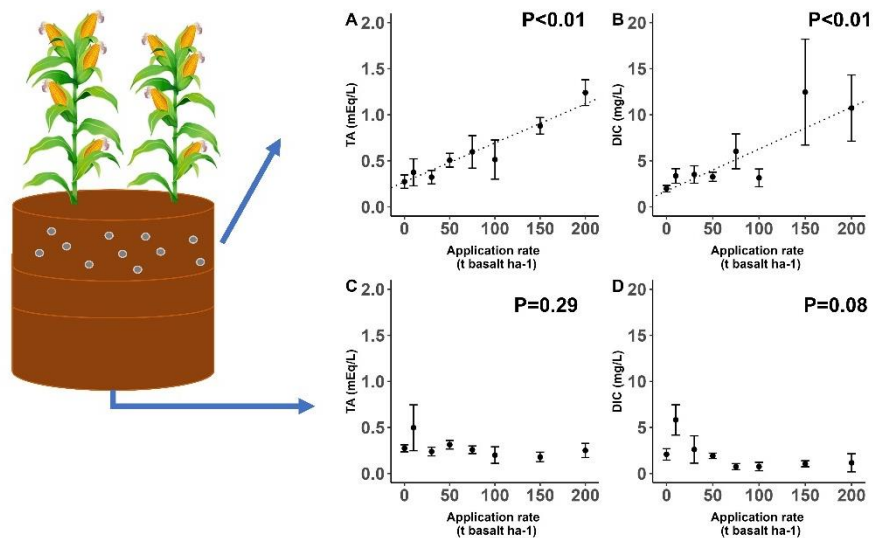
381 For SI_c and elemental stocks in plant biomass, soil pools and soil water export, a linear regression with basalt
382 application rate as a dependent variable was performed to test for a basalt effect. For measurements that were
383 repeated in time (pore water and leachate DIC and DOC compositions), a linear mixed model was used with basalt
384 and time as fixed factors and mesocosm as a random factor using the lme4 R package (version 1.1-33).
385 For measurements repeated in time, we assessed basalt x time interaction effects and discarded these if not
386 significant. All analyses were executed in R version 4.3.2. As an additional sensitivity analysis for the determination
387 of W_r using the slope of application rates approach described in the main text, we quantified W_r also for individual
388 application rates in **Fig. S13**.

389 To propagate uncertainty between basalt and controls in Figure 5, averages and standard errors for every replicated
390 application rate (0 or 50 t/ha) were determined. The average from the 50 t ha⁻¹ was subtracted with the average
391 from the control soil and $se = \sqrt{(se_control^2 + se_basalt^2)}$. For non-replicated application rates (10,30, 75,100,
392 150 and 200 t/ha, se=0) the measurement was subtracted from the control soil average and errors were also
393 propagated with $se = \sqrt{(se_control^2 + se_basalt^2)}$.

394 **3 Results**

395

396 Basalt amendment significantly increased DIC and TA in the top soil water (**Figure 4**). TA in soil water correlated
397 positively with DIC (R² = 0.68, p<0.01, **Fig. S10**). TA was thus generated in the basalt amended soil layer, yet we
398 did not observe DIC or TA increases with higher basalt application rates in water exported from the soil column at
399 60 cm depth (**Figure 4**). Temporal dynamics show that DIC in top soil pore water gradually increased in time with
400 higher basalt amendment, while DOC decreased in time with more basalt (**Fig. S7 and Table S4**).



402 **Figure 4:** Topsoil (0-20 cm) pore water (A) TA and (B) DIC concentrations. Export water (50 cm depth) (C) TA and
 403 (D) DIC concentrations. Values represent average concentrations +/- standard error across all sampling occasions
 404 over the 101-day experiment (n= 125, 44, 95 and 60 for pore water DIC, TA and leachate DIC and TA concentrations
 405 respectively). Significant trends are indicated with a dotted regression line. Raw data for TA and DIC in function of
 406 time is visualized in **Fig. S7(B,D)** and **Fig. S9(B,D)**.
 407
 408

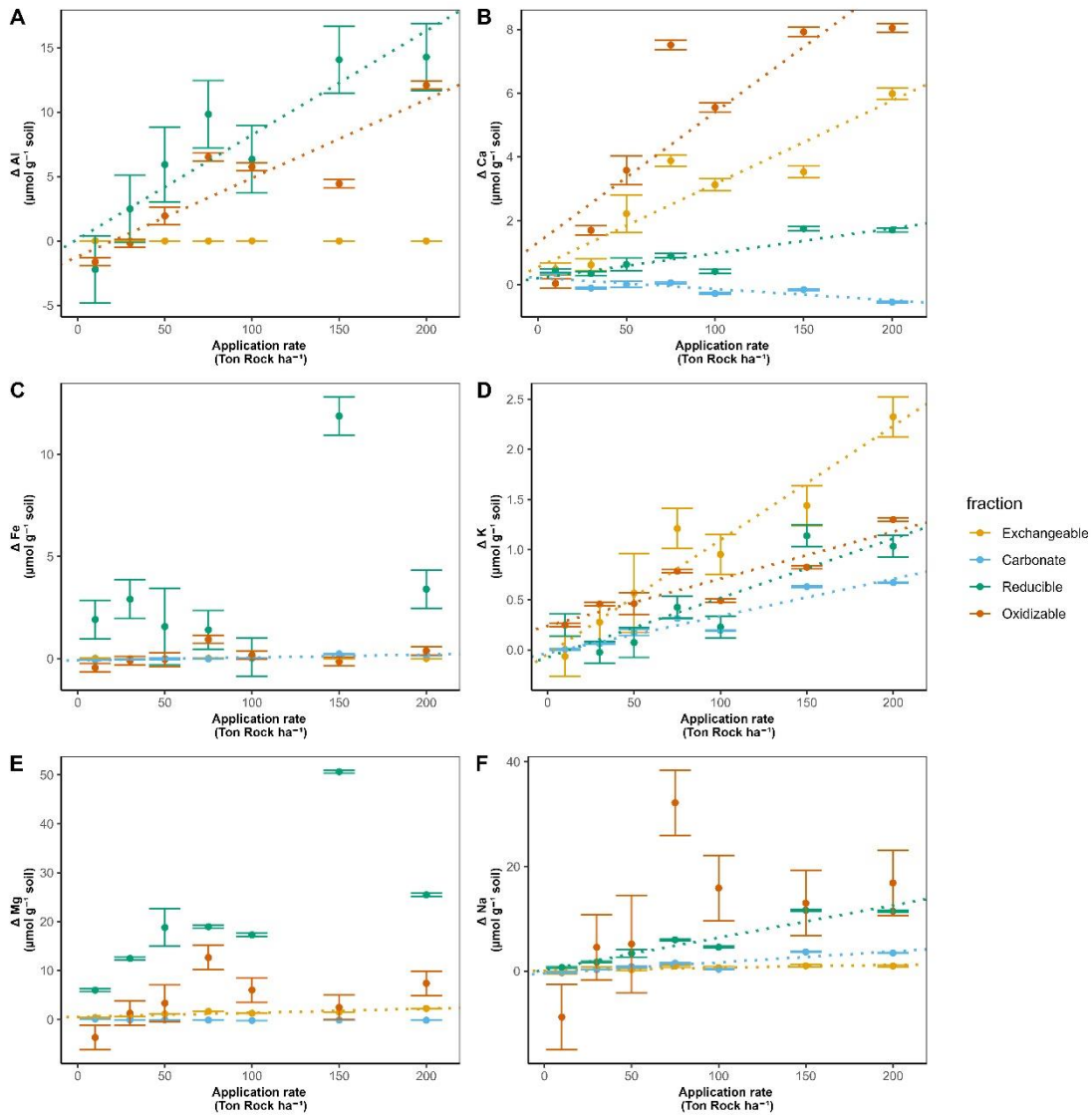
409 Overall, base cations were mostly retained in the top soil, where Ca significantly increased in the exchangeable,
 410 reducible and oxidizable pools with higher basalt addition. Only in the carbonate soil pool, Ca (and also Mg)
 411 significantly decreased with more basalt (**Figure 5 and 6**). With higher rock amendment, Mg accumulated in the
 412 top soil exchangeable pool ($p < 0.01$). The Mg accumulation in the reducible pool was higher compared to the
 413 exchangeable, but the slope was borderline significant for the reducible pool ($p = 0.07$) due to higher variability in Mg
 414 concentrations with increasing basalt amendment.

415 Changes in Na followed similar patterns as Mg, as also significantly more Na exchanged in top soil ($p = 0.02$) and a
 416 larger signal of reducible Na was found ($p < 0.01$). In contrast with divalent cations, monovalent cations increased in
 417 the carbonate fraction if basalt increased (**Figure 5 and 6**). With more basalt, Al is being found in association with
 418 the oxidizable and reducible fraction. Si increased only significantly in the oxidizable pool ($p = 0.04$) (**Fig. S15**).
 419 Increases in oxidizable Si, Ca, Al with higher basalt addition suggest the formation of mineral-associated organic
 420 matter.

421 In the soil layer just below the soil-basalt mixture (20-30 cm), the cations did not increase significantly in any of the
 422 measured soil pools and oxidizable Na, Fe and Mg decreased significantly (**Fig. S11, Figure 6**). We did not observe
 423 significant changes in any element with higher basalt amendment in the 30-50 cm soil layer (**Fig. S12**).

424

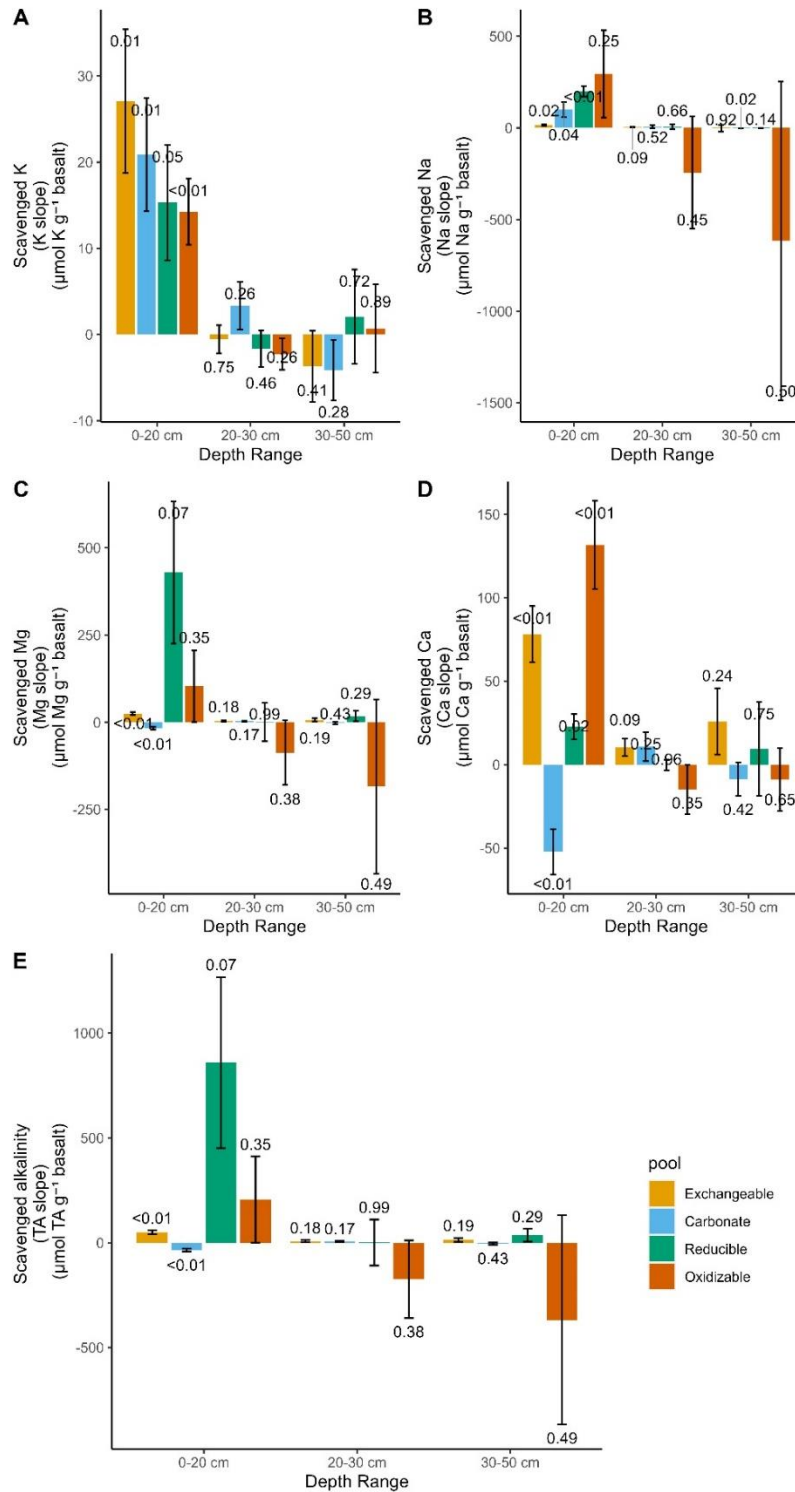
425



426
 427
 428 **Figure 5:** Change in topsoil (0-20 cm) elements relative to the control (corrected as in Equation 7), 101 days after
 429 basalt amendment, as a function of basalt application rate for (A) Al (B) Ca (C) Fe (D) K (E) Mg and (F) Na for four
 430 different soil pools. Dots and error bars represent averages and standard errors. For basalt application rates other
 431 than 50 t ha^{-1} , error bars correspond to those of the control soils, as these basalt treatments were not replicated
 432 and the data are shown as control-normalized results. Significant effects ($p < 0.05$) of basalt application rate on cation
 433 concentrations are indicated by dotted linear regression lines. Measurements were repeated on at least four
 434 samples per fraction for the control soils ($N \geq 4$ for each fraction) and $N=4$ for 50 t ha^{-1} treatment (fewer than 5
 435 replicates were available due to technical issues). Note that y-axes scales differ among subplots to better visualize
 436 small changes for some elements. Unnormalized (raw) data are presented in Fig. S19-21.

437
 438 From all significant element changes in soil pools, we calculate that 8.4%, 52.1% and 9.4% Of basalt Na, K and Ca
 439 were weathered while we do not observe an increase in Mg if we only consider significant ($p < 0.05$) slopes. If we
 440 consider all (also $p > 0.05$) regression slopes, the estimates become 48.0%, 10.6%, 9.35% for K, Ca and Mg, while
 441 Na did not increase in this approach (mass balance per element, see Fig. S23).

442



443
444

Figure 6: Equivalent alkalinity uptake 101 days after basalt amendment in different soil pools and depths. P-values of linear regressions are shown above and below bar plots of positive and negative changes respectively. Error bars represent the standard error that was derived from linear regression. Underlying regressions for slopes of TA scavenged by each pool and depth can be found in **Fig. S22**. Base cation changes in topsoil pore water are not included in this figure as we only include charge equivalent adsorbed by soil pools here, yet base cations in top soil pore water were negligible (see **Fig. S24**).

445
446
447
448
449
450
451
452
453
454
455
456

Base cations were not only scavenged by soils, but also by plants. Although two orders of magnitude smaller than in soil pools, TA scavenging by plants was higher than soil water exported TA and increased significantly with larger basalt amendment ($p < 0.01$) (**Figure 7**). The increase in base cation charges in plants was attributed to K (81%), Ca (11%) and Mg (8%).

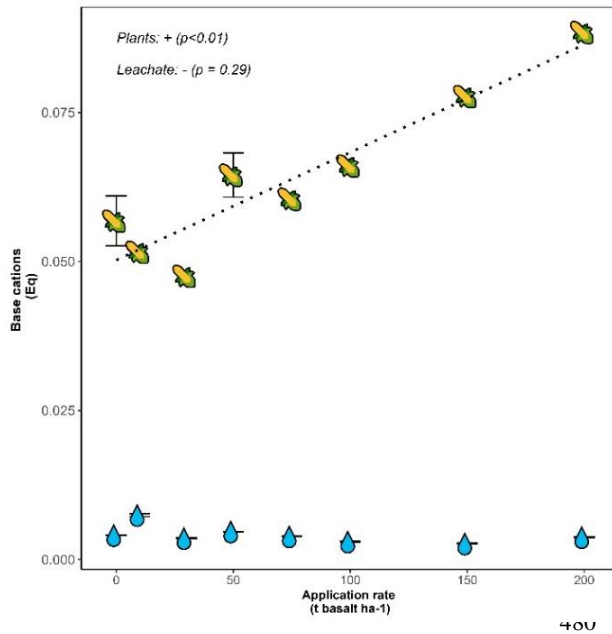


Figure 7: Base cation charge equivalents (Eq) per mesocosm after 101 days retained in maize plants (stems, leaves and maize ears), indicated with maize fruit symbols, and flushed with leaching water, indicated with droplets. Error bars represent averages and standard errors ($n=5$ for both control and 50 t ha^{-1} basalt replicates for plant measurements). For leachate TA, a total of 60 measurements were done in total at different dates. Na was not analyzed in plants and is thus not included in the harvested base cations. Errors on leachate TA were small and appear as horizontal lines within the droplets. Raw data for leachate TA measurements can be found in **Fig S9D**.

481 Converting the base cations to moles of equivalent TA and considering only the exchangeable pool as only soil
 482 cation reservoir we derive a log weathering rate of $-12.13 \pm 0.34 \text{ mol TA m}^{-2} \text{ rock s}^{-1}$ (**Table 4**). When we consider
 483 also the decrease in base cation equivalents in the carbonate pool, the mean estimate decreases to -12.23 mol TA
 484 $\text{m}^{-2} \text{ rock s}^{-1}$, translating into mean estimated potential inorganic CO_2 removals of $0.36\text{-}0.71 \text{ kg CO}_2 \text{ t}^{-1}$ basalt
 485 (assuming $\eta=0.5\text{-}1$). If we include all soil pools and non significant regressions the estimates becomes one order
 486 of magnitude higher, yet with substantial uncertainty.

487 **Table 4:** Overview of the Wr and potential inorganic CO_2 removal that can be quantified from changes in base
 488 cations in specific soil pools. Rows where (scavenged) TA increased significantly with increasing basalt amendment
 489 are indicated in bold.

Soil Pool	Depth	Reservoir	Log Wr (Log mol TA/m ² basalt /s)	CDR Potential* (kg CO ₂ /ton basalt) ($\eta = 0.5$)	CDR Potential* (kg CO ₂ /ton basalt) ($\eta = 1$)
/	/	Plant*	-12.93 ± 0.07	/	/
/	/	Leachate*	$Wr < 0$	/	/
Exchangeable	0-20cm	soil	-12.20 ± 0.41	1.10 ± 0.04	2.21 ± 0.07
Carbonate	0-20cm	soil	$Wr < 0$	-0.75 ± 0.03	-1.50 ± 0.06
Reducible	0-20cm	soil	-10.96 ± 0.21	18.91 ± 1.76	37.82 ± 3.51
Oxidizable	0-20cm	soil	-11.58 ± 0.43	4.53 ± 0.89	9.06 ± 1.77
Exchangeable	20-30cm	soil	-13.02 ± 0.29	0.17 ± 0.02	0.34 ± 0.04
Carbonate	20-30cm	soil	-13.17 ± 0.29	0.12 ± 0.02	0.23 ± 0.03
Reducible	20-30cm	soil	13.17 ± 50.43	0.02 ± 0.47	0.04 ± 0.95
Oxidizable	20-30cm	soil	$Wr < 0$	-3.82 ± 0.80	-7.56 ± 1.60
Exchangeable	30-50cm	soil	-12.76 ± 0.30	0.30 ± 0.04	0.61 ± 0.08
Carbonate	30-50cm	soil	$Wr < 0$	-0.10 ± 0.02	-0.21 ± 0.05
Reducible	30-50cm	soil	-12.34 ± 1.15	0.79 ± 0.13	1.58 ± 0.27
Oxidizable	30-50cm	soil	$Wr < 0$	-8.10 ± 2.15	-16.19 ± 4.31
Exchangeable	0-20	Exchangeable+plant+leachate	-12.13 ± 0.34	1.30 ± 0.04	2.21 ± 0.07
Exchangeable + Carbonate	0-20	Exchangeable+plant+leachate+ carbonate	-12.23 ± 1.05	0.36 ± 0.05	0.71 ± 0.10
All soil pools	All	All soil pools + plant + leachate	$-11.11 \pm 2.70^{**}$	13.17 ± 3.07	26.33 ± 6.13

490 *For leachates (which represents realized CDR) and also for plants there is no potential inorganic CO₂ removal in
491 this approach. ** Abs (Wr/standard error (Wr)*LN(10)) was used to propagate the error using the log10
492 transformation, resulting in substantial uncertainty for the Wr estimate of all pools.

493 **4. Discussion**

494 **4.1 Weathering rates and CO₂ removal**

495 EW is typically considered as a durable CDR pathway that removes CO₂ from the atmosphere by producing DIC
496 that is either transported to the ocean (Strefler et al., 2018) or precipitates as carbonates in the soil (Manning et al.,
497 2013). Here, we observe a clear weathering signal (a TA and DIC increase) in top soil pore water (**Figure 4**). These
498 TA and DIC increases in the pore water of amended top soil are consistent with recent findings (Holzer et al., 2023;
499 McDermott et al., 2024; Vienne et al., 2024). Increased DIC in basalt soils relative to controls may result from
500 enhanced plant DIC exudation or from mineral weathering; our dataset does not allow these effects to be separated.
501 DIC did however not leach from our soil columns within this experimental timeframe of 101 days.
502

503
504
505 Absence of substantial DIC leaching is in line with other short-term recent studies (Amann et al., 2020; Larkin et al.,
506 2022; Niron et al., 2024; Vienne et al., 2024). For example, the log Wr of approximately -13 mol TA m² s⁻¹ quantified
507 from DIC export after 1 year in a mesocosm trial with 220 ton ha⁻¹ olivine-rich rock (Amann et al., 2020) was about
508 three orders of magnitude lower than what would be expected from lab-scale weathering studies (roughly -10 mol
509 TA m² s⁻¹, (Palandri & Kharaka, 2004)). Vienne et al. (2024), amended soils with 100 ton basalt ha⁻¹ and quantified
510 a CDR from exported TA that was in the same order of magnitude as in the work of Amann et al. (2020). Although
511 the studies of Amann et al. (2020), Vienne et al. (2024) were relatively short (<= 1 year) and used a relatively low
512 water infiltration flux, also a longer (3 year duration) catchment-scale study in Malaysian oil palm plantations with
513 high annual rainfall (>2000 mm year⁻¹) detected no significant increase in TA leaching in the catchments (Larkin et
514 al., 2022). There may thus be a substantial delay for DIC leaching.

515
516 A DIC leaching delay can have multiple causes (**Figure 1**); A first possibility is pedogenic carbonate formation.
517 We observe that solid carbonates did not increase in our experiment, in contrast, SIC decreased in time. PHREEQC
518 calculations for our experiment suggest that dolomite and calcite were undersaturated, so that carbonate dissolution
519 was possible (**Fig. S17**). Saturation states are expected to be low in our experiment because control soil was
520 undersaturated and dissolved base cations accumulated in other soil pools than the carbonate pool (**Figure 5 and**
521 **6**). A decrease in SIC is in contrast with substantial SIC increases found after wollastonite rock amendment (Haque
522 et al., 2019, 2020). The observed SIC increase in the latter field study may be partly attributed to residual carbonates
523 from prior liming activities instead of new carbonate formation related to silicate weathering (Haque et al., 2020).
524 Thus, not all measured SIC may reflect new carbonate formation in the study of Haque et al. (2020). For short-term
525 basalt studies, using elemental C analysis, also no significant changes in SIC could be detected previously (Kelland

526 et al., 2020; Vienne et al., 2022, 2024). In contrast, in the study of Larkin et al. (2022), a relatively small SIC increase
527 was detected in amended soils, using carbonate pool extractions.

528
529 While TA was not exported or taken up by soil carbonates here and plant base cation losses were minor (**Table 4**)
530 it was retained in top soil where the exchangeable and reducible pools reduced solute TA. We expect cations to be
531 primarily associated with Fe- and Mn-(oxyhydr)oxides in the reducible pool and with organic matter in the oxidizable
532 pool, as supported by literature (Tessier et al., 1979); However, the extraction chemicals of this sequential extraction
533 scheme (hydroxylamine and H₂O₂) are known to have a limited specificity and may have also partially targeted
534 other mineral phases (such as clays) (Ryan et al., 2008), which could explain the elevated Si observed in the topsoil
535 pools (**Fig. S15**). In addition, the observed increase of aluminum in association with the reducible soil fraction
536 indicate the formation of secondary minerals. While we cannot pinpoint the exact Mg-phases formed in our soils,
537 our results do demonstrate substantial base cation retention in the soil and show that there can be more base cation
538 losses to soils than to the exchangeable pool alone.

539
540 Our estimate of log *W_r*, derived solely from significant increases in TA uptake at higher basalt amendment rates,
541 was approximately $-12 \text{ mol TA m}^{-2} \text{ s}^{-1}$. This estimate reflects changes in the exchangeable and carbonate soil
542 pools, plant uptake, and leachate composition. Notably, this value aligns with previous studies that estimated log *W_r*
543 values between -12 and -11 based on base cation depletion from the exchangeable pool alone (Kelland et al.,
544 2020; Reershemius et al., 2023; te Pas et al., 2023), as summarized in Vienne et al., (2024). Also in a batch leaching
545 experiment with 1mM CaCl₂ (designed to mimic soil solutions) the quantified log *W_r* of basalt was found to be -11
546 (Van Der Bauwhede et al., 2024).

547
548 Estimates from Buckingham et al. (2022), based only on leachates, gave a much lower log *W_r* of -15 , partly due to
549 low water infiltration rates. With a high infiltration flux (8000 mm/year), Amann et al. (2022) estimated log *W_r*
550 between -12.5 and -13.5 from basalt leachates. This highlights the importance of including scavenged alkalinity to
551 determine *W_r* in soils. When we also include non-significant regression slopes we derive a mean log *W_r* estimate
552 with substantial uncertainty (-11.11 ± 2.70) mol TA m⁻² s⁻¹. From individual application rates, we quantify log *W_r*
553 ranging between -11 and -10 (**Fig. S13**); These values are comparable to those observed in soil-free, laboratory-
554 scale basalt dissolution experiments conducted at circumneutral pH (Brantley et al., 2008; Gislason & Oelkers,
555 2003). They also approximate the dissolution rates of key mineralogical components in basalt (such as plagioclases
556 (between -12 and -9 for Na and Ca endmembers respectively) and augite (-11.97)) under room temperature and
557 neutral pH conditions (Gudbrandsson et al., 2011; Hermanska et al., 2022; Palandri & Kharaka, 2004a).

558

559 Although this and other experiments show relatively consistent weathering rates from exchangeable base cations
560 (comparable to those observed in lab-scale studies) we emphasize that, unlike laboratory conditions where base
561 cations remain far from equilibrium in excess water, soils experience solid-phase cation scavenging, which
562 promotes DIC degassing (**Figure 1**). From the sum of significant TA slopes we calculate a relatively low potential
563 inorganic CO₂ removal, equalling to approximately 0.36-0.71 kg CO₂ ton⁻¹ basalt or 0.018-0.036 tCO₂ ha⁻¹ for a
564 basalt application rate of 50 t ha⁻¹ (**Table 4**). Also the highest possible potential inorganic CO₂ removal realized
565 within this experimental timeframe is modest; Including also non-significant TA increases and assuming $\eta = 1$, the
566 potential inorganic CO₂ removal is quantified to be 26.33±6.13 kg CO₂ ton⁻¹ basalt (**Table 4**). We emphasize that
567 a potential inorganic CO₂ removal is a maximum inorganic CO₂ removal that can be realized with the delivered
568 amount of base cation weathering as strong acids associated with fertilizers (such as nitric acid and sulphuric acid),
569 or organic acids and not carbonic acid may have initially weathered silicate rock which does not lead to a CDR
570 within the soil system (McDermott et al., 2024; Taylor et al., 2021). Moreover, life-cycle emissions associated with
571 mining, grinding and transporting rock are typically of the same order of magnitude as our relatively low potential
572 inorganic CO₂ removal (Lefebvre et al., 2019).

573

574 Furthermore, for climate change mitigation, not only the amount of potential inorganic CO₂ removal is important,
575 but also the timescale at which this CDR is realized (Kanzaki et al., 2025). A mass balance of base cations indicates
576 that exported TA was negligible compared to base cation charges that were retained in the soil over the timeframe
577 of our experiment (101 days) (**Table 4**). As long as TA is retained in soil pools, inorganic CO₂ removal through DIC
578 export is delayed as equivalent amounts of protons have then been released into the soil water to maintain charge
579 balance (**Figure 1**). Realization of this delayed inorganic CO₂ removal depends on liberation of base cations from
580 these soil pools and their transport out of the soil, charge-balanced by HCO₃⁻. This export may take decades or
581 longer, depending on the circumstances (Kanzaki et al., 2025).

582

583 The realization of CDR may be further delayed through the formation of base cation bearing clay minerals. Clay
584 formation has previously been suggested for EW application based on changes in soil water Ge/Si ratios and Si
585 isotopes (Vienne et al., 2024) and also based on Li isotope measurements (Pogge von Strandmann et al., 2022).
586 These measurements indicated basalt induced clay formation, but it remains unclear what type of clays were formed
587 and hence what the effect on inorganic CO₂ removal may be. In the best case for the inorganic CO₂ removal time
588 lag, the formed clays are 1:1 phyllosilicates such as kaolinite that do not sequester base cations. In this case, DIC
589 leaching is only retarded by base cation exchange. Worst case for the inorganic CO₂ removal time lag, the formed
590 secondary minerals bear substantial amounts of base cations (e.g. chlorite, chrysotile, smectites, montmorillonites).
591 These clays exhibit a log W_r between -12 and -12.5 at neutral pH (Palandri & Kharaka, 2004), so that dissolution
592 within decadal timescales is unlikely (Bullock et al., 2022).

593

594 Although unfavourable for inorganic CO₂ removal, if base cation bearing secondary clay minerals would form, they
595 can increase SOC (Georgiou et al., 2022; Heckman et al., 2022; Steinwider et al., 2025). Georgiou et al. (2022)
596 refer to base-cation bearing clays (e.g. smectitic or illitic clays) as 'high-activity minerals' due to their higher SOM
597 stabilization capacity compared to secondary minerals that do not contain base cations (i.e., 'low-activity minerals',
598 with a lower CEC such as kaolinite). Both high- and low-activity minerals can adsorb DOC and form mineral-
599 associated organic matter-C (MAOM-C), which is believed to have a relatively high permanence (decades-
600 centuries) in soils (Lavallee et al., 2020). Besides mineral surface however, plant inputs can also limit SOC accrual.
601 In the latter case, SOC stocks can only increase if belowground plant C inputs increase, which could follow from
602 increases in exchangeable bases or pH (Haque et al., 2019; Shamshuddin et al., 2011). Nonetheless, increases in
603 decomposition can also stimulate SOC losses if rock dust increases soil pH (Klemme et al., 2022).

604

605 **4.2 Implications for monitoring inorganic CO₂ removal**

606

607 Different base cation monitoring strategies are possible. A first option is to quantify TA in soil water (Clarkson et
608 al., 2024). A disadvantage is however that soil water samples have to be sampled across the soil depth.
609 Alternatively, TA could be only monitored in top soil, yet then uncertain TA leaching models must be used (Kanzaki
610 et al., 2025). To calibrate TA leaching models, soil measurements in depth profiles could be used.

611

612 A first soil measurement approach is a total cation accounting approach, which quantifies the loss of base cations
613 from top soils (te Pas et al., 2025). However, this approach only focuses on the top soil and fails to account for
614 physical cation transport from top soils due to erosion or vertical feedstock transport via infiltration or bioturbation.
615 Alternatively, in a mobile/immobile tracer element approach (often named 'TiCat' by the EW community), cation
616 losses from amended top soils are quantified along with immobile tracers, which can account for cation losses
617 through bioturbation or erosion (Reershemius et al., 2023). Nonetheless the disadvantage of TiCat is that it does
618 not track potential TA scavenging (e.g. by organic matter or clays) at larger depth. Our potential inorganic CO₂
619 removal estimate will thus differ from a potential inorganic CO₂ removal estimate quantified using a TiCat approach.

620

621 Alternatively, entire depth profiles could be analyzed to spatially calibrate TA leaching models. Analysis of the
622 exchangeable soil pool is already a well-established method in EW research (Beerling et al., 2024; Reershemius et
623 al., 2023; Reynaert et al., 2023; Vienne et al., 2024). Adding also the carbonate, reducible and oxidizable soil pools
624 to the analysis could make base cation mass balancing more complete. These protocols could calibrate predictive
625 TA leaching models spatially. In addition there is an opportunity to quantify SOC and MAOM-C changes in the same
626 samples, which have recently gained traction in EW research due to their role in stabilizing SOM (Buss et al., 2024;
627 Sokol et al., 2024; Xu et al., 2024). Integration of these measurements can provide more accurate estimates of the

628 climate impact of EW, but should take into account the difference in permanence of inorganic and organic carbon
629 stocks.

630
631 However, this monitoring approach involves complexities such as feedstock correction, leaching solution strength
632 and soil heterogeneity. Although correcting for pre-weathered elements was crucial in this study, it assumes perfect
633 mixing based on a silicate-to-soil ratio. This correction was particularly significant for carbonate and reducible soil
634 pools, where for some base cations, over half of the cation increase with basalt amendment originated from
635 feedstock addition and not from weathering (**Fig. S18**). An alternative approach could involve creating time series
636 from sequential extraction data and quantifying base cation changes based on the change in time between multiple
637 measurements taken after rock amendment.

638
639 As discussed in the previous section, another key challenge is that the fate of base cations may remain uncertain
640 if strongly bound crystalline organo-minerals (see Lopez-Sangil & Rovira, 2013) form that are unextractable by the
641 Tessier scheme. Such processes may have contributed to the observed decrease in oxidizable elements at larger
642 depth, although this could also be an artefact of the applied extraction procedure. Pogge von Strandmann et al.
643 (2022) proposed substituting the H₂O₂ leaching step of the Tessier scheme with a dilute HCl leach, which is thought
644 to extract clays as well. Alternatively, post-extraction analysis of residual solids using techniques such as XRD or
645 QEMSCAN may be necessary to rigorously assess changes in rock mineralogy (Mason et al., 2022). Although deep
646 soil core sampling and extensive mineralogical analysis are resource-intensive and not feasible for large-scale
647 application, this monitoring strategy could be valuable during the initial adoption of EW in targeted 'measure-all'
648 experiments, as reliable TA leaching models require extensive calibration.

649

650 **5. Conclusions**

651 This study presents a detailed examination of EW and its effectiveness as a climate mitigation technique, revealing
652 both its potentials and limitations. A novel aspect of this work is the in-depth investigation of entire soil profiles for
653 base cations in different soil fractions, paired with soil water TA monitoring. We highlight the value of sequential
654 extractions as a method for monitoring base cations throughout soil profiles for calibrating TA leaching models.

655 Our findings indicate that basalt-based enhanced weathering may not immediately lead to the inorganic CO₂
656 removal previously anticipated in projections and IPCC reports (Babiker et al., 2022; Minx et al., 2018). We observed
657 rock weathering without inorganic CO₂ removal; despite the absence of DIC leaching or carbonate precipitation,
658 exchangeable bases increased with higher basalt amendments, demonstrating that rock weathering occurred.
659 Additionally, we observed a borderline significant but substantial increase in base cations in the reducible topsoil
660 pool with greater basalt application, which may further suppress TA leaching.

661 As base cation exchange increased with higher basalt amendments, we infer that greater application rates can
662 further delay the release of DIC from soil minerals to surface waters. However, in practice, EW is typically applied
663 at application rates below 30 t ha⁻¹. These lower, more practical rates may also enhance effectiveness of inorganic
664 CO₂ removal by reducing lag times for DIC release. It remains unclear if clays were formed here and whether EW
665 can deliver CDR within the urgent decadal timeframe needed to mitigate climate change. Despite its limitations for
666 short-term inorganic CO₂ removal, the generated secondary minerals and increased CEC could enhance plant
667 productivity and SOC retention in soils, contributing to long-term soil health, fertility, and potentially carbon
668 sequestration beyond inorganic pathways.

669 **Acknowledgements**

670 We thank Anne Cools, Steven Joosen and Anke De Boeck for their assistance with ICP-OES for sequential
671 extraction samples and Anthony De Schutter to characterize basalt using XRD. We thank DURUBAS to provide
672 basalt and provide the XRF material data sheet. We thank Tom Cox and Jasper Roussard for fruitful discussions.
673 We acknowledge the use of Microsoft Copilot and Ecosia AI to improve the English of this manuscript. This research
674 was supported by the Research Foundation— Flanders (FWO) [1S06325N], 1174925N] and [G000821N] (Biotic
675 controls of the potential of enhanced silicate weathering for land-based climate change mitigation). We also
676 acknowledge support of the UPSURGE project, which has received funding from the European Union's Horizon
677 2020 research and innovation program under grant agreement No 101003818.

678 **Author contribution**

679 AV: research conceptualization, data gathering, development methodology, data analysis and writing.
680 PF: conceptualized sequential extraction methodology, writing and discussion. JR: research conceptualization, data
681 gathering. TJS: writing and discussion. TR: writing and discussion. RP: data gathering, rock characterization and
682 writing. JH: writing and discussion. HN: development extraction methodology, writing and discussion. MPE:
683 elemental C measurements and proofreading. LSs: writing, development methodology and discussion. LB: writing
684 and discussion. SV: supervising research, conceptualization, writing and discussion.

685 **Data and code availability**

686 Data and code used in this manuscript are freely available at: <https://zenodo.org/records/15129984>

687 **Competing interests**

688 The authors have no competing interests to declare.

689 **References**

- 690 A. Gelman, & J. Hill. (2007). *Data analysis using regression and multilevel/hierarchical models*. Cambridge
691 University Press. https://moodle2.units.it/pluginfile.php/756424/mod_resource/content/1/gelman_hill_2007.pdf
- 692 Amann, T., & Hartmann, J. (2022). Carbon Accounting for Enhanced Weathering. *Frontiers in Climate*, 4(May), 1–
693 9. <https://doi.org/10.3389/fclim.2022.849948>
- 694 Amann, T., Hartmann, J., Hellmann, R., Pedrosa, E. T., & Malik, A. (2022). Enhanced weathering potentials—the
695 role of in situ CO₂ and grain size distribution. *Frontiers in Climate*, 4.
696 <https://doi.org/10.3389/fclim.2022.929268>
- 697 Amann, T., Hartmann, J., Struyf, E., De Oliveira Garcia, W., Fischer, E. K., Janssens, I., Meire, P., & Schoelynck,
698 J. (2020). Enhanced Weathering and related element fluxes - A cropland mesocosm approach.
699 *Biogeosciences*, 17(1), 103–119. <https://doi.org/10.5194/bg-17-103-2020>
- 700 Babiker, M., G. Berndes, K. Blok, B. Cohen, A. Cowie, O. Geden, V. Ginzburg, A. Leip, P. Smith, M. Sugiyama, F.
701 Y., & [P.R. Shukla, J. Skea, R. Slade, A. Al Khourdajie, R. van Diemen, D. McCollum, M. Pathak, S. Some,
702 P. Vyas, R. Fradera, M. Belkacemi, A. Hasija, G. Lisboa, S. Luz, J. Malley, (eds.)]. (2022). *Cross-sectoral
703 perspectives*. In *IPCC, 2022: Climate Change 2022: Mitigation of Climate Change. Contribution of Working*

- 704 *Group III to the Sixth Assessment Report of the Intergovernmental Panel on Climate Change.*
705 <https://doi.org/10.1017/9781009157926.005>
- 706 Barker, S. (2013). Dissolution of Deep-Sea Carbonates. In *Encyclopedia of Quaternary Science* (2nd ed., Vol. 2,
707 Issue 2002). Elsevier B.V. <https://doi.org/10.1016/B978-0-444-53643-3.00289-2>
- 708 Beerling, D. J., Epihov, D. Z., Kantola, I. B., Masters, M. D., Reershemius, T., Planavsky, N. J., & Reinhard, C. T.
709 (2024). Enhanced weathering in the US Corn Belt delivers carbon removal with agronomic benefits. *PNAS*,
710 1–10. <https://doi.org/10.1073/pnas>.
- 711 Bijma, J., Hagens, M., Hammes, J. S., Planavsky, N., Strandmann, P. A. E. P. Von, & Meeresforschung, H. P.-
712 (2026). *Reviews and syntheses: Carbon vs. cation based MRV of Enhanced Rock Weathering and the issue*
713 *of soil organic carbon*. 53–75.
- 714 Blume, H., Brümmer, G. W., Horn, R., & Kögel-knabner, I. (2016). *Scheffer/Schachtschabel soil science*. Springer.
715 <https://doi.org/10.1007/978-3-642-30942-7>
- 716 Brantley, S. L., White, A. F., & Kubicki, J. D. (2008). Kinetics of water-rock interaction. In *Kinetics of Water-Rock*
717 *Interaction* (Issue January). <https://doi.org/10.1007/978-0-387-73563-4>
- 718 Brown, I. C. (1943). A rapid method of determining exchangeable hydrogen and total exchangeable bases of soils.
719 In *Soil Science* (Vol. 56, Issue 5, pp. 353–357). <https://doi.org/10.1097/00010694-194311000-00004>
- 720 Buckingham, F. L., Henderson, G. M., Holdship, P., & Renforth, P. (2022). Applied Geochemistry Soil core study
721 indicates limited CO₂ removal by enhanced weathering in dry croplands in the UK. *Applied Geochemistry*,
722 147(October), 105482. <https://doi.org/10.1016/j.apgeochem.2022.105482>
- 723 Bullock, L. A., Yang, A., & Darton, R. C. (2022). Kinetics-informed global assessment of mine tailings for CO₂
724 removal. *Science of The Total Environment*, 808, 152111. <https://doi.org/10.1016/j.scitotenv.2021.152111>
- 725 Buss, W., Hasemer, H., Ferguson, S., & Borevitz, J. (2024). Stabilisation of soil organic matter with rock dust
726 partially counteracted by plants. *Global Change Biology*, 30(1), 1–14. <https://doi.org/10.1111/gcb.17052>
- 727 Clarkson, M. O., Larkin, C. S., Swoboda, P., Reershemius, T., Suhrhoff, T. J., Maesano, C. N., & Campbell, J. S.
728 (2024). A review of measurement for quantification of carbon dioxide removal by enhanced weathering in soil.
729 *Frontiers in Climate*, 6(June). <https://doi.org/10.3389/fclim.2024.1345224>
- 730 Dietzen, C., Harrison, R., & Michelsen-Correa, S. (2018). Effectiveness of enhanced mineral weathering as a carbon
731 sequestration tool and alternative to agricultural lime: An incubation experiment. *International Journal of*
732 *Greenhouse Gas Control*, 74(January), 251–258. <https://doi.org/10.1016/j.ijggc.2018.05.007>
- 733 Dzombak, D. A., & Morel, F. M. M. (1990). *Surface complexation modeling*. John Wiley & Sons (A Wiley-
734 Interscience Publication).
- 735 Fuss, S., Lamb, W. F., Callaghan, M. W., Hilaire, J., Creutzig, F., Amann, T., Beringer, T., De Oliveira Garcia, W.,
736 Hartmann, J., Khanna, T., Luderer, G., Nemet, G. F., Rogelj, J., Smith, P., Vicente, J. V., Wilcox, J., Del Mar
737 Zamora Dominguez, M., & Minx, J. C. (2018). Negative emissions - Part 2: Costs, potentials and side effects.
738 *Environmental Research Letters*, 13(6). <https://doi.org/10.1088/1748-9326/aabf9f>
- 739 Gao, Y., Lu, Y., Wu, M., Liang, E., Li, Y., Zhang, D., Yin, Z., Ren, X., Dai, Y., Deng, D., & Chen, J. (2016). Ability to
740 remove Na⁺ and retain K⁺ correlates with salt tolerance in two maize inbred lines seedlings. *Frontiers in Plant*
741 *Science*, 7(NOVEMBER2016), 1–15. <https://doi.org/10.3389/fpls.2016.01716>
- 742 Georgiou, K., Jackson, R. B., Vindušková, O., Abramoff, R. Z., Ahlström, A., Feng, W., Harden, J. W., Pellegrini, A.
743 F. A., Polley, H. W., Soong, J. L., Riley, W. J., & Torn, M. S. (2022). Global stocks and capacity of mineral-
744 associated soil organic carbon. *Nature Communications*, 13(1), 1–12. <https://doi.org/10.1038/s41467-022-31540-9>
- 746 Gislason, S. R., & Oelkers, E. H. (2003). Mechanism, rates, and consequences of basaltic glass dissolution: II. An
747 experimental study of the dissolution rates of basaltic glass as a function of pH and temperature. *Geochimica*
748 *et Cosmochimica Acta*, 67(20), 3817–3832. [https://doi.org/10.1016/S0016-7037\(00\)00176-5](https://doi.org/10.1016/S0016-7037(00)00176-5)
- 749 Gudbrandsson, S., Wolff-Boenisch, D., Gislason, S. R., & Oelkers, E. H. (2011). An experimental study of crystalline
750 basalt dissolution from 2pH11 and temperatures from 5 to 75°C. *Geochimica et Cosmochimica Acta*, 75(19),
751 5496–5509. <https://doi.org/10.1016/j.gca.2011.06.035>
- 752 Haque, F., Santos, R. M., & Chiang, Y. W. (2020). Optimizing Inorganic Carbon Sequestration and Crop Yield With
753 Wollastonite Soil Amendment in a Microplot Study. *Frontiers in Plant Science*, 11(July), 1–12.
754 <https://doi.org/10.3389/fpls.2020.01012>
- 755 Haque, F., Santos, R. M., Dutta, A., Thimmanagari, M., & Chiang, Y. W. (2019). Co-Benefits of Wollastonite

- 756 Weathering in Agriculture: CO₂ Sequestration and Promoted Plant Growth [Research-article]. *ACS Omega*,
757 4(1), 1425–1433. <https://doi.org/10.1021/acsomega.8b02477>
- 758 Heckman, K., Hicks Pries, C. E., Lawrence, C. R., Rasmussen, C., Crow, S. E., Hoyt, A. M., von Fromm, S. F., Shi,
759 Z., Stoner, S., McGrath, C., Beem-Miller, J., Berhe, A. A., Blankinship, J. C., Keiluweit, M., Marín-Spiotta, E.,
760 Monroe, J. G., Plante, A. F., Schimel, J., Sierra, C. A., ... Wagai, R. (2022). Beyond bulk: Density fractions
761 explain heterogeneity in global soil carbon abundance and persistence. *Global Change Biology*, 28(3), 1178–
762 1196. <https://doi.org/10.1111/gcb.16023>
- 763 Holzer, I. O., Nocco, M. A., & Houlton, B. Z. (2023). Direct evidence for atmospheric carbon dioxide removal via
764 enhanced weathering in cropland soil. *Environmental Research Communications*, 5(10).
765 <https://doi.org/10.1088/2515-7620/acfd89>
- 766 Janssens, I. A., Roobroeck, D., Sardans, J., Obersteiner, M., Peñuelas, J., Richter, A., Smith, P., Verbruggen, E.,
767 & Vicca, S. (2022). *Negative erosion and negative emissions : Combining multiple land-based carbon dioxide*
768 *removal techniques to rebuild fertile topsoils and enhance food production.*
- 769 Kalinichev, A. G., Iskrenova-Tchoukova, E., Ahn, W. Y., Clark, M. M., & Kirkpatrick, R. J. (2011). Effects of Ca²⁺
770 on supramolecular aggregation of natural organic matter in aqueous solutions: A comparison of molecular
771 modeling approaches. *Geoderma*, 169, 27–32. <https://doi.org/10.1016/j.geoderma.2010.09.002>
- 772 Kanzaki, Y., Planavsky, N. J., Zhang, S., Jordan, J., Suhrhoff, T. J., & Reinhard, C. T. (2025). Soil cation storage is
773 a key control on the carbon removal dynamics of enhanced weathering. *Environmental Research Letters*,
774 20(074055).
- 775 Katarzyna A. Kowalczyk, Thorben Amann, Jessica Strefler, M.-E., Vorrath, Jens Hartmann, Serena De Marco, Phil
776 Renforth, S., & Foteinis, E. K. (2024). Marine Carbon Dioxide Removal by alkalization should no longer be
777 overlooked. *Environmental Research Letters*, December 2016, 11–14.
- 778 Kelland, M. E., Wade, P. W., Lewis, A. L., Taylor, L. L., Sarkar, B., Andrews, M. G., Lomas, M. R., Cotton, T. E. A.,
779 Kemp, S. J., James, R. H., Pearce, C. R., Hartley, S. E., Hodson, M. E., Leake, J. R., Banwart, S. A., &
780 Beerling, D. J. (2020). Increased yield and CO₂ sequestration potential with the C4 cereal Sorghum bicolor
781 cultivated in basaltic rock dust-amended agricultural soil. *Global Change Biology*, 26(6), 3658–3676.
782 <https://doi.org/10.1111/gcb.15089>
- 783 Klemme, A., Rixen, T., Müller, M., Notholt, J., & Warneke, T. (2022). Destabilization of carbon in tropical peatlands
784 by enhanced weathering. *Communications Earth and Environment*, 3(1), 1–9.
785 <https://doi.org/10.1038/s43247-022-00544-0>
- 786 Larkin, C. S., Andrews, M. G., Pearce, C. R., Yeong, K. L., Beerling, D. J., Bellamy, J., Benedick, S., Freckleton, R.
787 P., Goring-harford, H., Sadekar, S., & James, R. H. (2022). Quantification of CO removal in a large-scale
788 enhanced weathering field trial on an oil palm plantation in Sabah , Malaysia. *Frontiers in Climate*.
789 <https://doi.org/10.3389/fclim.2022.959229>
- 790 Lavallee, J. M., Soong, J. L., & Cotrufo, M. F. (2020). Conceptualizing soil organic matter into particulate and
791 mineral-associated forms to address global change in the 21st century. *Global Change Biology*, 26(1), 261–
792 273. <https://doi.org/10.1111/gcb.14859>
- 793 Lefebvre, D., Goglio, P., Williams, A., Manning, D. A. C., Carlos, A., Azevedo, D., Bergmann, M., Meersmans, J.,
794 & Smith, P. (2019). Assessing the potential of soil carbonation and enhanced weathering through Life Cycle
795 Assessment : A case study for Sao Paulo State , Brazil. *Journal of Cleaner Production*, 233, 468–481.
796 <https://doi.org/10.1016/j.jclepro.2019.06.099>
- 797 Lopez-Sangil, L., & Rovira, P. (2013). Sequential chemical extractions of the mineral-associated soil organic matter:
798 An integrated approach for the fractionation of organo-mineral complexes. *Soil Biology and Biochemistry*, 62,
799 57–67. <https://doi.org/10.1016/j.soilbio.2013.03.004>
- 800 Manning, D. A. C., Renforth, P., Lopez-Capel, E., Robertson, S., & Ghazireh, N. (2013). Carbonate precipitation in
801 artificial soils produced from basaltic quarry fines and composts: An opportunity for passive carbon
802 sequestration. *International Journal of Greenhouse Gas Control*, 17, 309–317.
803 <https://doi.org/10.1016/j.ijggc.2013.05.012>
- 804 Mason, J., Lin, E., Grono, E., & Denham, T. (2022). QEMSCAN® analysis of clay-rich stratigraphy associated with
805 early agricultural contexts at Kuk Swamp, Papua New Guinea. *Journal of Archaeological Science: Reports*,
806 42(February), 103356. <https://doi.org/10.1016/j.jasrep.2022.103356>
- 807 Matylda Hermanska , Martin J. Voigt, Chiara Marieni, Julien Declercq, E. O. (2022). *A comprehensive and internally*
808 *consistent mineral dissolution rate database : Part I : Primary silicate minerals and glasses.* 597(July 2021).
809 <https://doi.org/10.1016/j.chemgeo.2022.120807>
- 810 McDermott, F., Bryson, M., Magee, R., & van Acken, D. (2024). Enhanced weathering for CO₂ removal using

- 811 carbonate-rich crushed returned concrete; a pilot study from SE Ireland. *Applied Geochemistry*, 169(June),
812 106056. <https://doi.org/10.1016/j.apgeochem.2024.106056>
- 813 Minx, J. C., Lamb, W. F., Callaghan, M. W., Fuss, S., Hilaire, J., Creutzig, F., Amann, T., Beringer, T., De Oliveira
814 Garcia, W., Hartmann, J., Khanna, T., Lenzi, D., Luderer, G., Nemet, G. F., Rogelj, J., Smith, P., Vicente
815 Vicente, J. L., Wilcox, J., & Del Mar Zamora Dominguez, M. (2018). Negative emissions - Part 1: Research
816 landscape and synthesis. *Environmental Research Letters*, 13(6). <https://doi.org/10.1088/1748-9326/aabf9b>
- 817 Morse, J. W., Arvidson, R. S., & Lüttge, A. (2007). Calcium carbonate formation and dissolution. *Chemical Reviews*,
818 107(2), 342–381. <https://doi.org/10.1021/cr050358j>
- 819 Navarre-Sitchler, A., & Brantley, S. (2007). Basalt weathering across scales. *Earth and Planetary Science Letters*,
820 261(1–2), 321–334. <https://doi.org/10.1016/j.epsl.2007.07.010>
- 821 Niron, H., Vienne, A., Frings, P., Poetra, R., & Vicca, S. (2024). Exploring the synergy of enhanced weathering and
822 *Bacillus subtilis*: A promising strategy for sustainable agriculture. *Global Change Biology*, 30(9), 1–18.
823 <https://doi.org/10.1111/gcb.17511>
- 824 Öquist, M. G., Wallin, M., Seibert, J., Bishop, K., & Laudon, H. (2009). Dissolved Inorganic Carbon Export Across
825 the Soil / Stream Interface and Its Fate in a Boreal Headwater Stream. *Environmental Science & Technology*,
826 43(19), 7364–7369.
- 827 Palandri, J. L., & Kharaka, Y. K. (2004). A compilation of rate parameters of water-mineral interaction kinetics for
828 application to geochemical modeling. *USGS Open File Report, 2004–1068*, 71. [http://www.dtic.mil/cgi-](http://www.dtic.mil/cgi-bin/GetTRDoc?Location=U2&doc=GetTRDoc.pdf&AD=ADA440035)
829 [bin/GetTRDoc?Location=U2&doc=GetTRDoc.pdf&AD=ADA440035](http://www.dtic.mil/cgi-bin/GetTRDoc?Location=U2&doc=GetTRDoc.pdf&AD=ADA440035)
- 830 Poeplau, C., Don, A., Six, J., Kaiser, M., Benbi, D., Chenu, C., Cotrufo, M. F., Derrien, D., Gioacchini, P., Grand,
831 S., Gregorich, E., Griepentrog, M., Gunina, A., Haddix, M., Kuzyakov, Y., Kühnel, A., Macdonald, L. M.,
832 Soong, J., Trigalet, S., ... Nieder, R. (2018). Isolating organic carbon fractions with varying turnover rates in
833 temperate agricultural soils – A comprehensive method comparison. *Soil Biology and Biochemistry*,
834 125(April), 10–26. <https://doi.org/10.1016/j.soilbio.2018.06.025>
- 835 Pogge von Strandmann, P. A. E., Liu, X., Liu, C. Y., Wilson, D. J., Hammond, S. J., Tarbuck, G., Aristilde, L.,
836 Krause, A. J., & Fraser, W. T. (2022). Lithium isotope behaviour during basalt weathering experiments
837 amended with organic acids. *Geochimica et Cosmochimica Acta*, 328, 37–57.
838 <https://doi.org/10.1016/j.gca.2022.04.032>
- 839 Power, I. M., Hatten, V. N. J., Guo, M., Rausis, K., & Klyn-hesselink, H. (2025). Are enhanced rock weathering rates
840 overestimated? A few geochemical and mineralogical pitfalls. *Frontiers in Climate*, 6(January), 1–9.
841 <https://doi.org/10.3389/fclim.2024.1510747>
- 842 Reershemius, T., Kelland, M. E., Jordan, J. S., Davis, I. R., D'Ascanio, R., Calderon-Asael, B., Asael, D., Suhrhoff,
843 T. J., Epihov, D. Z., Beerling, D. J., Reinhard, C. T., & Planavsky, N. J. (2023). Initial Validation of a Soil-
844 Based Mass-Balance Approach for Empirical Monitoring of Enhanced Rock Weathering Rates. *Environmental*
845 *Science and Technology*, 57(48), 19497–19507. <https://doi.org/10.1021/acs.est.3c03609>
- 846 Renforth, P. (2012). The potential of enhanced weathering in the UK. *International Journal of Greenhouse Gas*
847 *Control*, 10, 229–243. <https://doi.org/10.1016/j.ijggc.2012.06.011>
- 848 Renforth, Phil. (2019). The negative emission potential of alkaline materials. *Nature Communications*, 10(1).
849 <https://doi.org/10.1038/s41467-019-09475-5>
- 850 Renforth, Phil., & Henderson, G. (2017). Assessing ocean alkalinity for carbon sequestration. *Reviews of*
851 *Geophysics*, 55(3), 636–674. <https://doi.org/10.1002/2016RG000533>
- 852 Reynaert, S., Vienne, A., De Boeck, H. J., D'Hose, T., Janssens, I., Nijs, I., Portillo-Estrada, M., Verbruggen, E.,
853 Vicca, S., & Poblador, S. (2023). Basalt addition improves the performance of young grassland monocultures
854 under more persistent weather featuring longer dry and wet spells. *Agricultural and Forest Meteorology*,
855 340(July), 109610. <https://doi.org/10.1016/j.agrformet.2023.109610>
- 856 Rijnders, J., Vienne, A., & Vicca, S. (2025). Effects of basalt, concrete fines, and steel slag on maize growth and
857 toxic trace element accumulation in an enhanced weathering experiment. *Biogeosciences*, 22(12), 2803–
858 2829. <https://doi.org/10.5194/bg-22-2803-2025>
- 859 Robert A. Berner. (1991). A model for Atmospheric CO₂ over phanerozoic time. *American Journal of Science*, 291,
860 339–376.
- 861 Rowley, M. C., Grand, S., & Verrecchia, É. P. (2018). Calcium-mediated stabilisation of soil organic carbon.
862 *Biogeochemistry*, 137(1–2), 27–49. <https://doi.org/10.1007/s10533-017-0410-1>
- 863 Ryan, P. C., Hillier, S., & Wall, A. J. (2008). Stepwise effects of the BCR sequential chemical extraction procedure

- 864 on dissolution and metal release from common ferromagnesian clay minerals: A combined solution chemistry
865 and X-ray powder diffraction study. *Science of the Total Environment*, 407(1), 603–614.
866 <https://doi.org/10.1016/j.scitotenv.2008.09.019>
- 867 Schindlbacher, A., Beck, K., Holzheu, S., & Borcken, W. (2019). Inorganic Carbon Leaching From a Warmed and
868 Irrigated Carbonate Forest Soil. *Frontiers in Forest and Global Change*, 2(August), 1–13.
869 <https://doi.org/10.3389/ffgc.2019.00040>
- 870 Shamshuddin, J., Anda, M., Fauziah, C. I., & Omar, S. S. R. (2011). Growth of cocoa planted on highly weathered
871 soil as affected by application of basalt and/or compost. *Communications in Soil Science and Plant Analysis*,
872 42(22), 2751–2766. <https://doi.org/10.1080/00103624.2011.622822>
- 873 Smith, P., Davis, S. J., Creutzig, F., Fuss, S., Minx, J., Gabrielle, B., Kato, E., Jackson, R. B., Cowie, A., Kriegler,
874 E., Van Vuuren, D. P., Rogelj, J., Ciais, P., Milne, J., Canadell, J. G., McCollum, D., Peters, G., Andrew, R.,
875 Krey, V., ... Yongsung, C. (2016). Biophysical and economic limits to negative CO₂ emissions. *Nature Climate
876 Change*, 6(1), 42–50. <https://doi.org/10.1038/nclimate2870>
- 877 Sokol, N. W., Sohng, J., Moreland, K., Slessarev, E., Goertzen, H., Schmidt, R., Samaddar, S., Holzer, I., Almaraz,
878 M., Geoghegan, E., Houlton, B., Montañez, I., Pett-Ridge, J., & Scow, K. (2024). Reduced accrual of mineral-
879 associated organic matter after two years of enhanced rock weathering in cropland soils, though no net losses
880 of soil organic carbon. *Biogeochemistry Letters*, 167(8), 989–1005. <https://doi.org/10.1007/s10533-024-01160-0>
- 882 Steinwider, L., Boito, L., Frings, P. J., Niron, H., Rijnders, J., de Schutter, A., Vienne, A., & Vicca, S. (2025).
883 Beyond Inorganic C: Soil Organic C as a Key Pathway for Carbon Sequestration in Enhanced Weathering.
884 *Global Change Biology*, 31(7). <https://doi.org/10.1111/gcb.70340>
- 885 Steinwider, L., Boito, L., Frings, P., Niron, H., Rijnders, J., De Schutter, A., Vienne, A., & Vicca, S. (2025). Beyond
886 inorganic carbon : Soil organic carbon as key pathway for carbon sequestration in Enhanced Weathering.
887 *Global Change Biology*.
- 888 Strefler, J., Amann, T., Bauer, N., Kriegler, E., & Hartmann, J. (2018). Potential and costs of carbon dioxide removal
889 by enhanced weathering of rocks. *Environmental Research Letters*, 13(3). <https://doi.org/10.1088/1748-9326/aaa9c4>
- 891 Suarez, D. L., & Grieve, C. M. (1988). Predicting cation ratios in corn from saline solution composition. *Journal of
892 Experimental Botany*, 39(5), 605–612. <https://doi.org/10.1093/jxb/39.5.605>
- 893 Swoboda, P., Döring, T. F., & Hamer, M. (2021). Remineralizing soils? The agricultural usage of silicate rock
894 powders: A review. *Science of the Total Environment*, 807(150976), 18.
895 <https://doi.org/10.1016/j.scitotenv.2021.150976>
- 896 Takaya, Y., Wu, M., & Kato, Y. (2019). Unique environmental conditions required for dawsonite formation:
897 Implications from dawsonite synthesis experiments under alkaline conditions. *ACS Earth and Space
898 Chemistry*, 3(2), 285–294. <https://doi.org/10.1021/acsearthspacechem.8b00121>
- 899 Taylor, L., Driscoll, C., Groffman, P., Rau, G., Blum, J., & Beerling, D. (2021). Increased carbon capture by a silicate-
900 treated forested watershed affected by acid deposition. *Biogeosciences Discussions*, 1–29.
901 <https://doi.org/10.5194/bg-2020-288>
- 902 te Pas, E. E. E. M., Chang, E., Marklein, A. R., Comans, R. N. J., & Hagens, M. (2025). Accounting for retarded
903 weathering products in comparing methods for quantifying carbon dioxide removal in a short-term enhanced
904 weathering study. *Frontiers in Climate*, 2029(February), 1–10. <https://doi.org/10.3389/fclim.2024.1524998>
- 905 te Pas, E. E. E. M., Hagens, M., & Comans, R. N. J. (2023). Assessment of the enhanced weathering potential of
906 different silicate minerals to improve soil quality and sequester CO₂. *Frontiers in Climate*, 4.
907 <https://doi.org/10.3389/fclim.2022.954064>
- 908 Tessier, A., Campbell, P. G. C., & Bisson, M. (1979). Sequential Extraction Procedure for the Speciation of
909 Particulate Trace Metals. *Analytical Chemistry*, 51(7), 844–851. <https://doi.org/10.1021/ac50043a017>
- 910 Tipping, E., & Hurley, M. A. (1992). A unifying model of cation binding by humic substances. *Geochimica et
911 Cosmochimica Acta*, 56(10), 3627–3641. [https://doi.org/10.1016/0016-7037\(92\)90158-F](https://doi.org/10.1016/0016-7037(92)90158-F)
- 912 Van Bemmelen, J. (1890). Über Die Bestimmung Des Wassers, Des Humus, Des Schwefels, Der in Den Colloidalen
913 Silikaten Gebundenen Kieselsäure, Des Mangans U. S. W. Im Ackerboden. *Die Landwirtschaftlichen
914 Versuchs-Stationen*, 37, 279–290.
- 915 Van Der Bauwhede, R., Muys, B., Vancampenhout, K., & Smolders, E. (2024). Geoderma Accelerated weathering
916 of silicate rock dusts predicts the slow-release liming in soils depending on rock mineralogy , soil acidity , and
917 test methodology. *Geoderma*, 441(November 2023), 116734.

- 918 <https://doi.org/10.1016/j.geoderma.2023.116734>
- 919 Van Straaten, P. (2006). Farming with rocks and minerals: Challenges and opportunities. *Anais Da Academia*
920 *Brasileira de Ciencias*, 78(4), 731–747. <https://doi.org/10.1590/S0001-37652006000400009>
- 921 Vienne, A., Frings, P., Poblador, S., Steinwider, L., Rijnders, J., Schoelynck, J., Vinduskova, O., & Vicca, S. (2024).
922 Earthworms in an enhanced weathering mesocosm experiment : Effects on soil carbon sequestration , base
923 cation exchange and soil CO₂ efflux. *Soil Biology and Biochemistry*, 199(June), 109596.
924 <https://doi.org/10.1016/j.soilbio.2024.109596>
- 925 Vienne, A., Poblador, S., Portillo-estrada, M., Hartmann, J., Ijehon, S., Wade, P., & Vicca, S. (2022). Enhanced
926 Weathering Using Basalt Rock Powder : Carbon Sequestration , Co-benefits and Risks in a Mesocosm Study
927 With *Solanum tuberosum*. *Frontiers in Climate*, 4(May), 1–14. <https://doi.org/10.3389/fclim.2022.869456>
- 928 Wolf-Gladrow, D. A., Zeebe, R. E., Klaas, C., Körtzinger, A., & Dickson, A. G. (2007). Total alkalinity: The explicit
929 conservative expression and its application to biogeochemical processes. *Marine Chemistry*, 106(1-2 SPEC.
930 ISS.), 287–300. <https://doi.org/10.1016/j.marchem.2007.01.006>
- 931 Xu, T., Yuan, Z., Vicca, S., Goll, D. S., Li, G., Lin, L., Chen, H., Bi, B., Chen, Q., Li, C., Wang, X., Wang, C., Hao,
932 Z., Fang, Y., & Beerling, D. J. (2024). Enhanced silicate weathering accelerates forest carbon sequestration
933 by stimulating the soil mineral carbon pump. *Global Change Biology*, 30(8), 1–17.
934 <https://doi.org/10.1111/gcb.17464>
- 935 Zhang, S., Planavsky, N. J., Katchinoff, J., Raymond, P. A., Kanzaki, Y., Reershemius, T., & Reinhard, C. T. (2022).
936 River chemistry constraints on the carbon capture potential of surficial enhanced rock weathering. *Limnology*
937 *and Oceanography*, 67(S2), S148–S157. <https://doi.org/10.1002/lno.12244>
- 938